eLife

Reviewed Preprint
v1 • April 20, 2026
Not revised

For correspondence:
houximiao@nwsuaf.edu.cn

Competing interests: No competing interests declared

Funding: See page 26

Reviewing editor: Chang Liu, Johns Hopkins University, United States

Multifaceted Functional Complexity of SARS-CoV-2 Helicase Nsp13 Underlies Its Integrated Motor and Remodeling Activities

Hai-Hong Li, Jia-Li Hou, Xue-Yang Yu, Jie Jin, Xi-Miao Hou
College of Life Sciences, Northwest A&F University, Yangling, China

eLife Assessment

This study characterizes several novel activities of SARS-CoV-2 helicase nsp13, providing **valuable** insights into potentially new functions of this essential RNA-processing enzyme in the virus life cycle. However, the experimental evidence to support the authors' claims is **incomplete**. In addition, the placement of the polyhistidine affinity tag on nsp13 may cause artifacts, raising concerns about the interpretation of the results.

https://doi.org/10.7554/eLife.110731.1.sa3

Abstract

SARS-CoV-2 nonstructural protein 13 (Nsp13) is a superfamily 1 helicase essential for viral replication. Although its canonical ATP-dependent unwinding activity is well established, the broader functional repertoire of Nsp13 remains unclear. Here, we show that Nsp13 encodes a high degree of complexity by acting as a tunable nucleic acid remodeler that integrates motor and non-motor activities within a single protein. Nsp13 operates in multiple mechanistically distinct regimes, including a canonical ATP-dependent helicase mode and a Mg^{2+}-primed, ATP-independent remodeling state capable of destabilizing short duplexes, hairpins, and G-quadruplexes. Mg^{2+} binding allosterically stabilizes a compact RecA1–RecA2 configuration, priming the enzyme for ATP-independent remodeling. Unwinding polarity is substrate-dependent, with duplexes supporting bidirectional remodeling, whereas G-quadruplexes are preferentially resolved in the 5'→3' direction. Beyond strand separation, Nsp13 also exhibits robust strand annealing and nucleic acid chaperone activities. Cofactors, substrate topology, and enzyme concentration dynamically regulate these activities. Together, our findings establish Nsp13 as a highly integrated nucleic acid remodeling system and reveal how a single viral helicase switches between motor-driven and remodeling-dominated states to meet the structural demands of replication and transcription.

Introduction

The COVID-19 pandemic, caused by Severe Acute Respiratory Syndrome Coronavirus 2 (SARS-CoV-2), has posed an unprecedented global health challenge. Although the acute phase has largely subsided, continued viral evolution and the long-term burden of post-acute sequelae (Long COVID) underscore the persistent threat posed by coronaviruses. As of December 2025, the World Health Organization has reported more than 779 million confirmed cases and over 7.1 million deaths worldwide, highlighting the ongoing need to understand the molecular mechanisms that underpin coronavirus replication and adaptability.

SARS-CoV-2 possesses large, positive-sense RNA genome (~30 kb) that fold into highly structured and dynamic architectures[1], including stem-loops, pseudoknots[2], and G-quadruplexes (G4s)[3–5]. These RNA structures play critical roles in regulating replication, transcription, translation, and genome packaging[6]. However, the structural flexibility of RNA makes it prone to kinetic trapping in non-functional conformations[7]. This inherent complexity creates a strong dependence on nucleic acid remodeling factor that can both resolve obstructive structures and assist the formation of functional ones[8, 9]. Viral helicases and chaperones fulfill these essential functions through distinct mechanisms[10]: helicases use NTP hydrolysis to unwind structured nucleic acids, whereas chaperones promote folding or restructuring without consuming ATP.

Among the 16 nonstructural proteins encoded by SARS-CoV-2[11], Nsp13 is the only helicase and is indispensable for viral replication[12]. Nsp13 belongs to the superfamily 1b (SF1b) helicases and has been classically described as a 5'→3' ATP-dependent motor[13, 14]. Notably, Nsp13 ranks among the most conserved coronavirus proteins[15], differing by only a single amino acid between SARS-CoV and SARS-CoV-2 (V570I), and retaining >99% identity across major viral variants[16, 17]. Such exceptional conservation suggests stringent functional constraints and implies a central, possibly multifaceted role within the viral replication–transcription complex (RTC)[18–20].

Consistent with this view, Nsp13 has traditionally been positioned at the leading edge of the RTC, where it unwinds upstream RNA, removes secondary-structure barriers, and facilitates template switching during discontinuous transcription[12, 21–23]. However, accumulating evidence indicates that its behavior cannot be fully captured by a canonical helicase model. SARS-CoV Nsp13 has been reported to exhibit ADP-stimulated chaperone-like activity that destabilizes DNA structures through transient collisions[24], while SARS-CoV-2 Nsp13 can resolve RNA stem–loops via an ATP-independent mechanism[25]. Most strikingly, recent cryo-EM analyses of the native RTC suggest that Nsp13 unwinds newly synthesized RNA duplexes with an apparent 3'→5' polarity[26]. These findings point to a functional complexity that may exceed the conventional definition of a helicase.

Despite above intriguing findings, key questions remain unanswered. How ATP-independent remodeling by Nsp13 is activated and regulated remains unclear. Whether unwinding polarity is an intrinsic property of the enzyme or an emergent feature dictated by substrate geometry remains unclear. Moreover, its potential to recognize and remodel G4s prevalent in both host and viral genomes has not been explored.

In this study, through an integrated approach combining biochemistry, biophysics, and structural modeling, we uncover an unexpectedly high degree of functional integration within SARS-CoV-2 Nsp13. Beyond its canonical ATP-dependent helicase activity, Nsp13 engages a divalent cation–activated, ATP-independent remodeling mode that supports strand unwinding, annealing, and chaperone-like restructuring across diverse nucleic acid substrates, including duplexes, hairpins, and G4s. These activities are dynamically tuned by cofactor availability, substrate topology, and enzyme concentration, enabling Nsp13 to switch between motor-driven and remodeling-dominated states. By establishing how multiple, mechanistically distinct nucleic acid transactions are integrated within a single viral helicase, our work expands the conceptual framework for helicase function and highlights new principles for understanding—and potentially targeting—viral replication machineries.

Results

Nsp13 is a broad-spectrum nucleic acid-binding protein

SARS-CoV-2 Nsp13 adopts a conserved helicase architecture, comprising an N-terminal zinc-binding domain (ZBD), two RecA-like domains (1A and 2A), a bridging 1B domain, and an auxiliary stalk domain that connects the ZBD to the helicase core (Figure 1A; PDB: 7nio)[28]. The ATP-binding pocket lies at the cleft between domains 1A and 2A, whereas the nucleic-acid–binding groove spans domains 1A, 2A, and 1B. To biochemically characterize the protein, we expressed and purified recombinant SARS-CoV-2 Nsp13 (hereafter referred to as Nsp13) in *E. coli* (Figure 1B). LC–MS/MS analysis confirmed protein identity, achieving 87% sequence coverage with

>93% of peptide–spectrum matches uniquely assigned to SARS-CoV-2 Nsp13 (Table S2). Size-exclusion chromatography further indicated that Nsp13 elutes as a single symmetric peak consistent with a monomeric state in solution (Figure 1C).

Fluorescence anisotropy assays showed that Nsp13 binds a broad spectrum of DNA and RNA substrates with low- to mid-nanomolar affinities (Figure 1D; Table S3). ATP hydrolysis was not required for substrate engagement, as the ATPase-deficient K288R mutant [29] displayed binding affinities indistinguishable from the wild-type protein (Figure 1E–F). Specifically, Nsp13 bound single-stranded DNA (Kd = 15.8 ± 1.3 nM) and RNA (Kd = 19.9 ± 0.9 nM) with comparable affinity, but preferentially recognized structured RNA elements, including a 5'-tailed RNA hairpin (Kd = 10.9 ± 0.4 nM) and an RNA G4 (Kd = 11.6 ± 0.8 nM). Notably, most binding curves were better fitted by a Hill model with coefficients >1 (Figure S1), indicating cooperative binding behavior[27].

Collectively, these findings establish SARS-CoV-2 Nsp13 as a potent, broad-specificity nucleic acid–binding helicase, with a marked preference for structured RNA elements.

Divalent cations activate a novel ATP-independent DNA unwinding mode

To comprehensively assess the unwinding capability of Nsp13, we initially employed a 16-bp duplex DNA substrate with a 14-nucleotide 5'overhang (5'Oh$_{S14D16}$), consistent with its reported 5'→3' polarity[30]. Surprisingly, in the absence of ATP, Nsp13 efficiently unwound this substrate in a concentration-dependent manner when Mg^{2+} was present (5 mM; Figure 2A). This activity exhibited a clear dependence on Mg^{2+} concentration over a broad range (0–20 mM; Figure 2B) and was retained in an N-terminal His-tag–deleted construct, excluding tag-dependent artifacts (Figure S2).

This ATP-independent activity was not restricted to Mg^{2+}. Other divalent cations, including Ca^{2+} and Mn^{2+}, also activated Nsp13 with a relative efficacy of Mg^{2+} > Ca^{2+} > Mn^{2+} (Figure 2C). Together, these results reveal a previously unrecognized DNA-remodeling activity of Nsp13 that is strongly activated by divalent cations and does not require ATP. This cation-driven unwinding mode represents a mechanistically distinct operational state of the enzyme, markedly different from its canonical ATP-fueled helicase cycle.

Mg^{2+} allosterically stabilizes Nsp13 and primes a non-processive remodeling conformation

To elucidate the mechanism underlying Mg^{2+}-activated ATP-independent unwinding, we first examined whether Mg^{2+} directly destabilizes the duplex substrate. FRET melting assays revealed that 5 mM Mg^{2+} significantly stabilized the double-stranded DNA, increasing its melting temperature (T_m) from 49 °C to 57.7 °C (Figure S3A). Addition of Nsp13 up to 1.8 μM only induced a marginal decrease in T_m (55.5-56.4°C; Figure S3B-C), indicating that the observed unwinding is not attributable to substrate destabilization. Moreover, fluorescence anisotropy measurements showed that Mg^{2+} modestly weakened Nsp13's binding affinity for a 5'-overhang DNA substrate, with the Kd increasing from 265.5 ± 0.41 nM (0 mM Mg^{2+}) to 434.4 ± 4.23 nM (0.5 mM Mg^{2+}) (Figure S3D), ruling out enhanced binding as the driver of unwinding.

We next asked whether Mg^{2+} directly alters the structural stability and conformational state of Nsp13. Circular dichroism (CD) thermal unfolding experiments revealed that Mg^{2+} modestly stabilized Nsp13 at near-physiological temperatures, despite no significant change in overall thermostability (Figure 2D-E). In the absence of Mg^{2+}, unfolding began at approximately 37 °C, whereas the onset of unfolding shifted to ∼41 °C in the presence of Mg^{2+}, suggesting that Mg^{2+} helps maintain a more compact conformation under near-physiological conditions.

AlphaFold3 structural modeling provided further mechanistic insight. As shown in Figure S4A, the predicted Nsp13 structure closely matched the known crystal structure, supporting the validity of our modeling. Notably, Mg^{2+} binding promotes a more compact arrangement between the RecA1

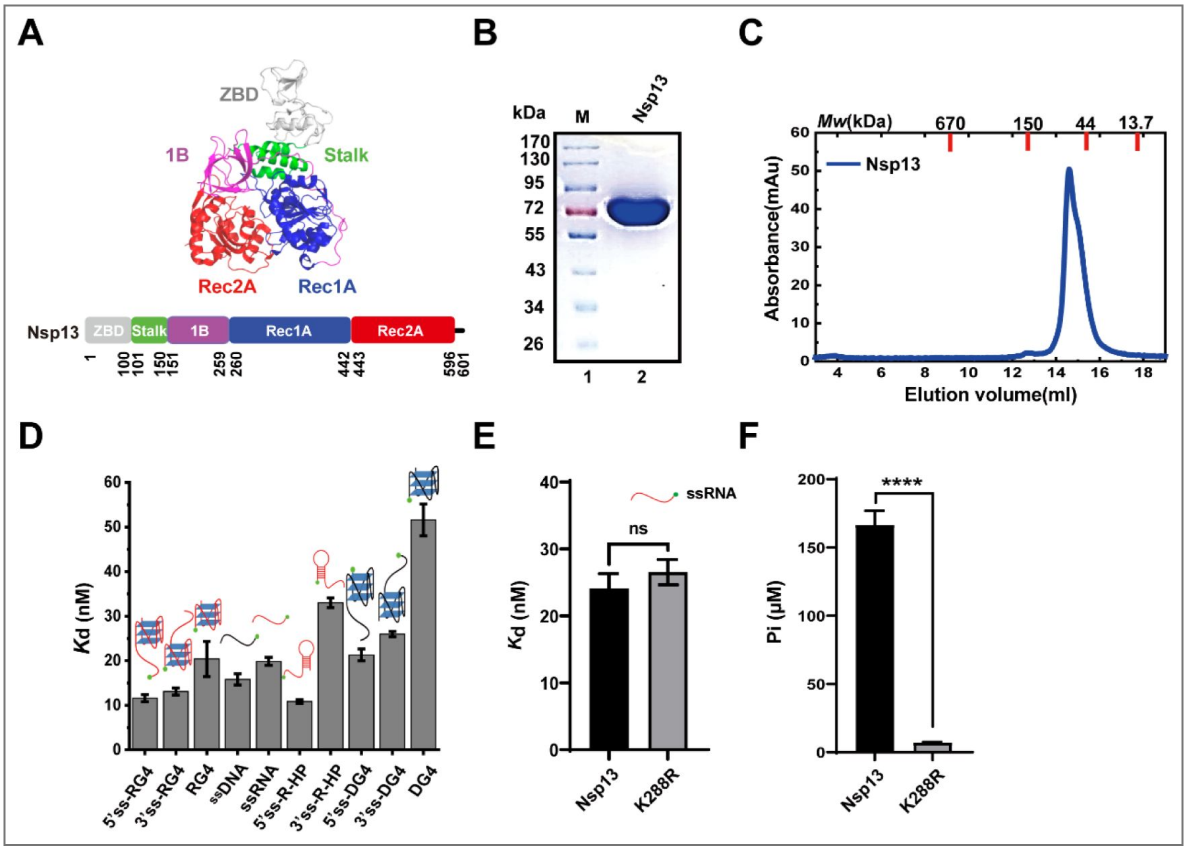

Figure 1. **Structural features and biochemical characterization of SARS-CoV-2 Nsp13.**

(A) Domain architecture and structure of Nsp13 from PDB (7nio). (B) SDS-PAGE analysis of purified Nsp13. (C) Size-exclusion chromatography (SEC) profile of Nsp13, indicating a monomeric state in solution. (D) Equilibrium dissociation constants (Kd) of Nsp13 with various nucleic acid substrates. (E) Binding affinity of the ATPase-deficient mutant K288R compared to wild-type Nsp13. (F) ATPase activities of wild-type Nsp13 and K288R mutant in the presence of ssRNA. Data are presented as mean ± SD (n=3). Statistical significance was determined by unpaired Student's t-test for comparisons between two groups, or one-way ANOVA followed by Tukey's HSD test for comparisons involving more than two groups; ns, P>0.05, P < 0.05, p < 0.01, P<0.001, P<0.0001 (apply to all figures).

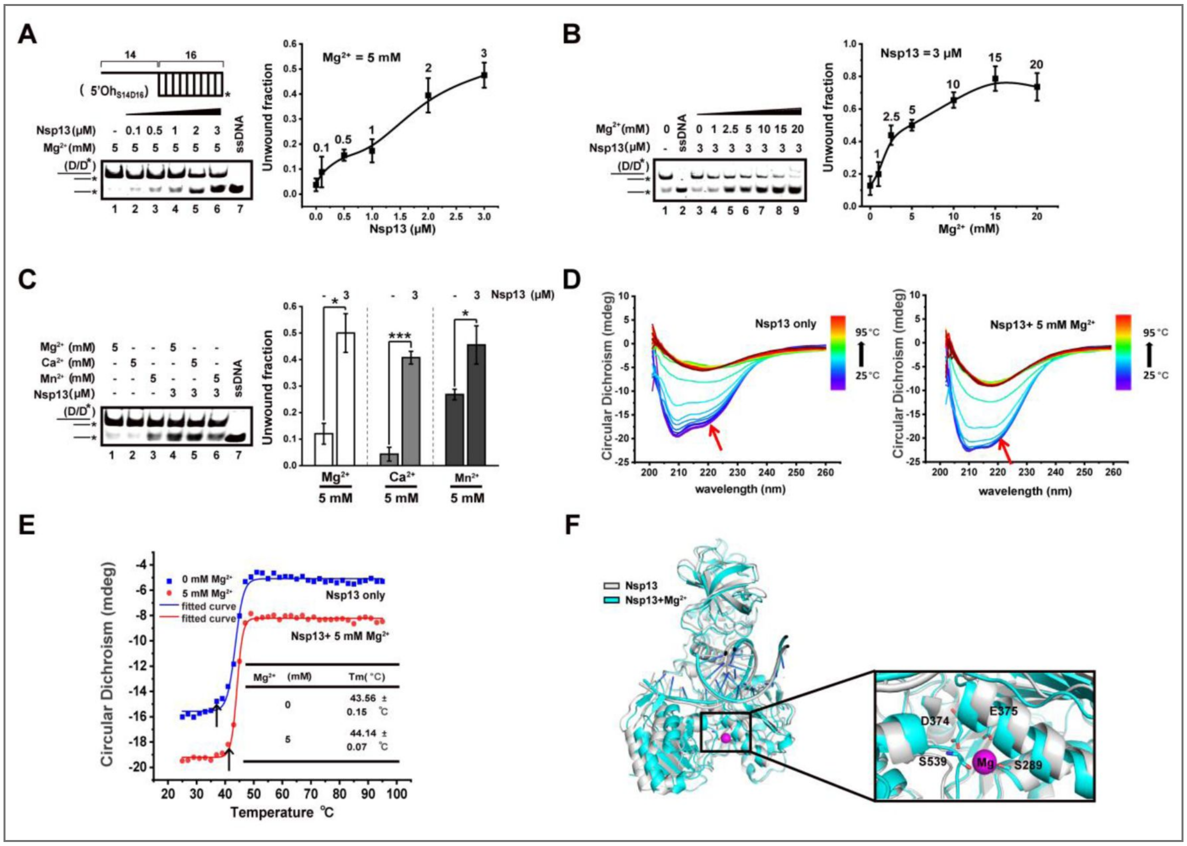

Figure 2. Divalent cations activate ATP-independent DNA unwinding and allosterically stabilize Nsp13.

(A) Schematic of the 5'-overhang DNA substrate with * denoting the FAM label (5'Oh$_{S14D16}$) and EMSA showing Nsp13-mediated, concentration-dependent unwinding in the presence of 5 mM Mg^{2+} without ATP (DNA substrate: 40 nM). Right panel: quantification of unwound DNA fraction. (B) EMSA and quantification illustrating the effect of Mg^{2+} concentration (0–20 mM) on ATP-independent DNA unwinding. (C) EMSA and quantification comparing the activation of DNA unwinding by different divalent cations (Mg^{2+}, Ca^{2+}, Mn^{2+}). (D) CD spectra of Nsp13 in the absence and presence of 5 mM Mg^{2+}. (E) Thermal denaturation curves of Nsp13 monitored by CD at 222 nm. (F) AlphaFold3-predicted structural models of the Nsp13–RNA fork complex, highlighting Mg^{2+}-induced compaction between the RecA1 and RecA2 domains (RNA was selected for modeling due to its higher prediction confidence relative to DNA). Data are presented as mean ± SD (n=3).

and RecA2 domains, primarily through interactions involving several key amino acids (Figure 2F), offering a structural explanation for the thermal stabilization observed in CD melting. This model of cation-driven allosteric stabilization is further supported by the conformational behavior of Nsp13 in the presence of ADP-Mg^{2+}, where the protein adopted a more compact state with specific residues potentially involved in Mg^{2+} coordination (Figure S4B).

Together, these findings establish Mg^{2+} as an allosteric effector that stabilizes Nsp13 and promotes a compact, low-processivity conformational state. This Mg^{2+}-primed state provides a mechanistic basis for the ATP-independent unwinding mode and highlights how Nsp13 can toggle between distinct functional regimes depending on the availability of nucleotides and cations.

Energy availability governs switching between distinct DNA remodeling modes and polarities

We next investigated the role of nucleotide binding and hydrolysis. We found that the non-hydrolyzable ATP analog AMP-PNP could stimulate dsDNA unwinding similarly as ATP and more effectively than Mg^{2+} alone (Figure 3A-B). Remarkably, K288R exhibited even greater unwinding activity in the presence of ATP than wild-type Nsp13 under either ATP or AMP-PNP conditions. AlphaFold3 modeling suggests that this enhancement may reflect a more tightly closed RecA1–RecA2 conformation in the ATP–Mg^{2+}–bound K288R mutant (Figure S5). These findings demonstrate that ATP binding, even without hydrolysis, is sufficient to induce a conformational state in Nsp13 that is highly proficient in DNA unwinding.

The ATP-independent unwinding mode, however, has limited processivity. When challenged with a more stable 24-bp dsDNA substrate, Nsp13 failed to unwind it in the presence of Mg^{2+} alone (Figure 3C), requiring ATP hydrolysis for this more demanding task. This indicates that while metal ion activation enables basal remodeling activity, processive unwinding of stable substrates depends on energy derived from ATP hydrolysis. Furthermore, the ATP-dependent activity was sensitively regulated by the ATP/Mg^{2+} balance. At a fixed ATP concentration (1 mM), excess Mg^{2+} beyond 1 mM strongly inhibited unwinding (Figure S6A). Conversely, maintaining a 1:1 ATP/Mg^{2+} ratio preserved robust unwinding efficiency across a range of ATP concentrations (1-5 mM; Figure S6B), underscoring the critical balance between these cofactors for optimal Nsp13 function.

Having defined two distinct unwinding regimes—an ATP-independent, cation-activated mode with limited processivity and a canonical ATP hydrolysis–dependent mode capable of processive strand separation—we next asked whether these modes impose a fixed directionality on DNA unwinding. Nsp13 has traditionally been classified as a strict 5'→3' helicase based primarily on assays employing substrates with 5' single-stranded overhangs. To test whether this polarity represents an intrinsic constraint or a context-dependent property, we examined Nsp13 activity on duplex DNA substrates bearing a 3' single-stranded overhang.

As a boundary condition, blunt-ended duplex DNA was not unwound under either ATP-independent or ATP-dependent conditions, confirming the requirement for a single-stranded loading region (Figure 3D). In contrast, when a substrate containing a 12-bp duplex region and a 3' overhang was used, we observed robust unwinding in the presence of Mg^{2+} alone, indicating that the cation-activated, ATP-independent mode is sufficient to support efficient 3'→5' DNA unwinding (Figure 3E-F). Addition of ATP produced a comparable extent of unwinding, suggesting functional redundancy between the ATP-independent and ATP-dependent modes on this substrate. Similar results were obtained with a more stable substrate containing a 16-bp duplex region (Figure S6C).

Together, these results establish that DNA unwinding by Nsp13 is governed by two orthogonal parameters: the energetic state of the enzyme and the geometry of the DNA substrate. Mg^{2+} binding induces a compact conformation that primes Nsp13 for basal strand remodeling but supports only limited processivity. In contrast, ATP binding alone is sufficient to promote a highly active unwinding conformation, while ATP hydrolysis provides the energy required to sustain processive separation of more stable duplexes. Importantly, neither the cation-activated nor the

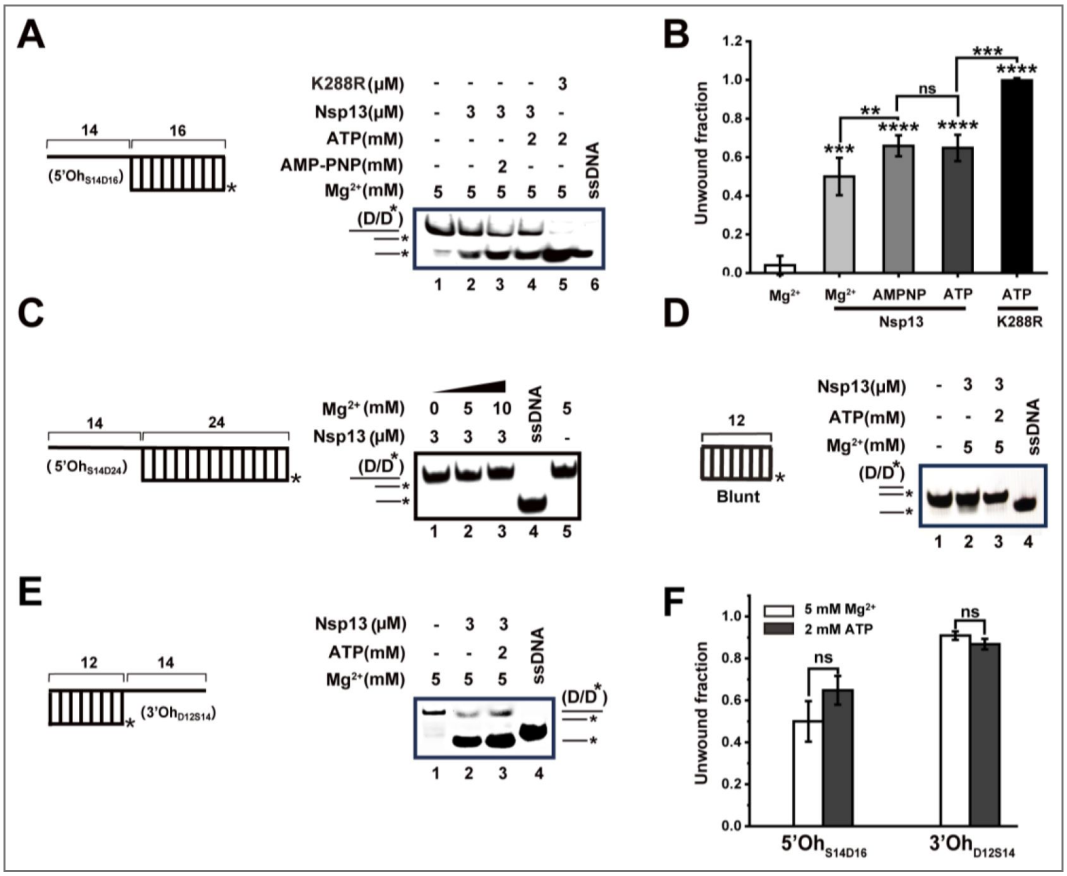

Figure 3. **Energy- and substrate-dependent DNA unwinding by Nsp13.**

(A–B) EMSA and quantification comparing Nsp13-mediated duplex DNA unwinding under different nucleotide and Mg^{2+} conditions. K288R was included as a control to assess the contribution of ATP hydrolysis. (C) Schematic of the 24-bp DNA substrate unwound only in the presence of Mg^{2+}. (D) Blunt-ended duplex DNA cannot be unwound by Nsp13 under either ATP-independent or ATP-dependent conditions. (E) Schematic of a 3'-overhang DNA substrate (3'Oh_{D12S14}) and EMSA showing Nsp13-mediated unwinding in the presence of 5 mM Mg^{2+}, either in the absence or presence of 2 mM ATP. (F) Quantification of unwound DNA fraction. Data represent mean ± SD (n = 3).

ATP-dependent mode enforces a strict polarity constraint. Instead, unwinding directionality emerges from the substrate context, revealing pronounced mechanistic plasticity that enables Nsp13 to unwind duplex DNA in either direction. This functional flexibility provides an essential framework for interpreting recent structural studies showing that, within the native RTC, Nsp13 operates with 3'→5' polarity to unwind newly synthesized RNA duplexes[26].

RNA substrates reveal a Mg^{2+}- and concentration-dependent remodeling regime distinct from DNA

Having established the ATP-independent unwinding activity of Nsp13 on DNA, we sought to determine if a similar mechanism applies to RNA substrates.

A key finding was the narrow optimal range for Mg^{2+} in facilitating RNA unwinding. When assayed using an RNA-fork substrate (Figure 4A, upper panel), Nsp13 (2 μM) exhibited negligible unwinding activity in the absence of Mg^{2+}, and the substrate showed signs of instability under Mg^{2+}-free condition (Figure S7A). Strikingly, the introduction of 0.5 mM Mg^{2+} enabled a pronounced unwinding activity, with efficiency peaking at ~30% (Figure 4A-B). K288R exhibited a comparable level of activity at this Mg^{2+} concentration (Figure 4C-D, lane 5), confirming that this pathway does not require ATP hydrolysis. However, this activation was highly specific, as increasing the Mg^{2+} concentration to 1 mM markedly suppressed the activity to 15.4% (Figure S7A, Figure 4B). This sharp decline stands in stark contrast to the positive correlation between Mg^{2+} concentration and unwinding efficiency observed for duplex DNA (Figure 2B), highlighting a nucleic acid-type-specific regulatory mechanism.

The interplay between nucleotide binding and the cation activation also differed for RNA. While AMP-PNP stimulated dsDNA unwinding, it did not enhance dsRNA unwinding beyond the level achieved by 0.5 mM Mg^{2+} alone (Figure 4C-D). Intriguingly, at 1 mM Mg^{2+} where ATP-independent mode is insignificant, at a low protein concentration (80 nM), a striking difference emerged: ATP-dependent unwinding (60%) overwhelmingly dominated, showing a ~13-fold enhancement over the minimal activity achieved with Mg^{2+} only (4.7%) (Figure 4E-F). The ATP hydrolysis-deficient mutant K288R showed no differential activity across treatments (Figure S7B, Figure 4F), confirming that it is ATP hydrolysis that serves as the key and potent trigger for this highly efficient RNA unwinding mode at low enzyme concentrations.

We further characterized the concentration dependence of ATP-dependent RNA unwinding at 1 mM Mg^{2+} (Figure 4G). Strikingly, it shows triphasic pattern-activation, inhibition, and restoration (Figure 4H), consistent with that was observed for the ATP-independent pathway (Figure S7C). At low Nsp13 concentrations (≤ 160 nM), robust RNA unwinding was observed. However, at an intermediate concentration of 0.4 μM, the unwinding activity was significantly inhibited. Further increasing the Nsp13 concentration beyond 1.6 μM led to a pronounced recovery of unwinding efficiency (Figure 4H). Control experiments confirmed that this inhibitory phase is governed by the absolute concentration of Nsp13 rather than the protein-to-substrate ratio (Figure S8), suggesting an intrinsic property of Nsp13 at this specific concentration range. This nonlinear behavior was specific to RNA substrates, as DNA unwinding exhibited a standard, cooperative increase with protein concentration under identical conditions (Figure S9).

Altogether, Nsp13 employs a distinct and sophisticated strategy to unwind RNA, characterized by a narrow Mg^{2+} optimum and a complex concentration-dependent regulatory mechanism. This behavior, which is qualitatively different from its action on DNA, suggests that RNA substrates induce specific conformational changes or functional states in Nsp13, leading to a unique regulatory mechanism tailored for RNA processing.

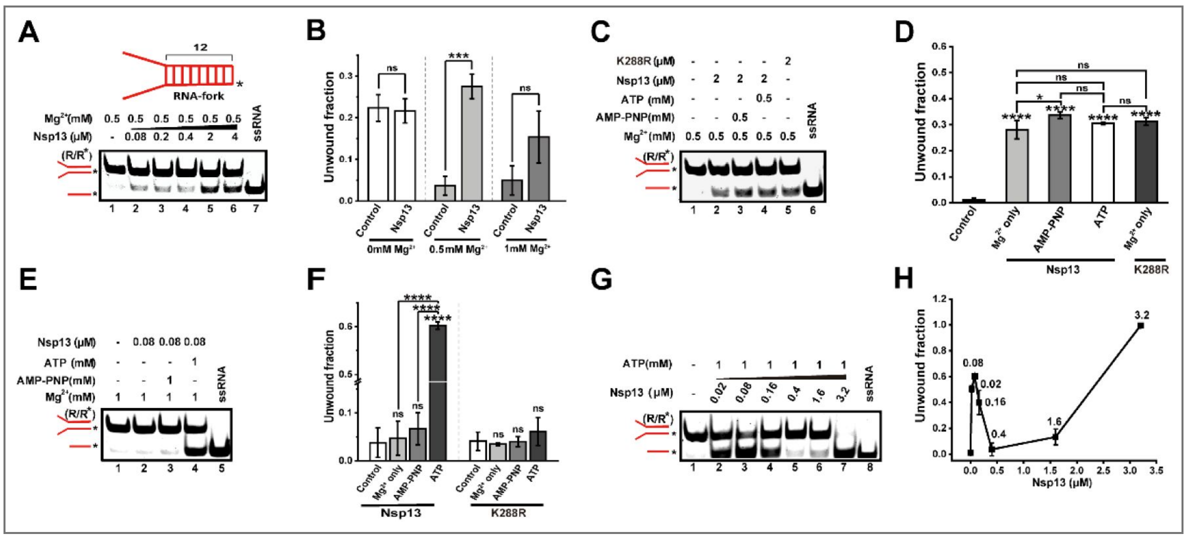

Figure 4. **Mg²⁺ activates ATP-independent and -dependent RNA unwinding with unique sensitivity and concentration dependence.**

(A) Schematic of the RNA-fork substrate and EMSA showing RNA unwinding at 0.5 mM Mg^{2+} without ATP. (B) Quantification of unwinding efficiency by 2 μM Nsp13 at 0, 0.5, and 1 mM Mg^{2+}. (C-D) EMSA and quantification of RNA unwinding under different ATP conditions. (E-F) Comparison of wild-type Nsp13 and K288R mutant unwinding at low protein concentration (80 nM). (G-H) EMSA and quantification showing triphasic concentration dependence of ATP-dependent RNA unwinding at 1 mM Mg^{2+}. RNA substrate concentration: 40 nM. Data are presented as mean ± SD (n=3).

Nsp13 resolves G4 structures through dual ATP-dependent and -independent pathways

Having established that Nsp13 exhibits versatile nucleic acid remodeling activities on conventional duplexes, we next sought to investigate its capacity to resolve highly stable G4 structures. Given the prevalence of putative G4-forming sequences in both the human and SARS-CoV-2 genomes and their potential regulatory roles in viral replication[31, 32], we evaluated Nsp13's activity on human telomeric DNA G4 (DG4) [33]and a conserved viral RNA G4 (RG-1) [6]using a gel-based unfolding assay (Figure 5A).

Strikingly, Nsp13 unwound the blunt-ended DG4 structure even in the absence of ATP, with efficiency increasing in a concentration-dependent manner (Figure 5B). The addition of ATP further enhanced the unfolding proportion (Figure 5C, D), demonstrating that Nsp13 possesses dual ATP-independent and ATP-dependent G4 resolving activities. Figure 5E–G further showed that Nsp13 efficiently unwound the 5'-overhang DG4 in an ATP-dependent manner, but showed much weaker activity on the 3'-overhang substrate. These results indicate that, although Nsp13 can switch polarity in duplex DNA unwinding, its G4 unfolding activity predominantly follows a 5'→3' direction.

This dual-mode capability also extended to RNA G4 structures. Nsp13 efficiently unfolded the SARS-CoV-2 genomic RG-1 through both ATP-independent and ATP-dependent mechanisms (Figure 5H-J). Intriguingly, the ATP-independent activity surpassed the ATP-dependent one across a broad protein concentration range (Figure 5J). This preference likely reflects intrinsic stability differences: RG-1 forms a relatively less stable two-layer G4 [34]that is more easily disrupted by direct binding–induced destabilization (chaperone mode), whereas the more stable three-layer DG4 requires processive, ATP-driven unwinding. Consistent with duplex RNA results (Figure 4G-H), RG-1 unfolding was inhibited at high Nsp13 concentrations (Figure S10), indicating a shared concentration-dependent regulatory behavior.

These findings significantly expand the functional repertoire of Nsp13, positioning it as a dual-mode nucleic acid remodeler capable of resolving complex G4 structures prevalent in both host and viral genomes. This activity, fine-tuned by ATP availability and substrate architecture, likely plays a crucial role in managing genomic stability and facilitating the progression of the viral RTC through G-rich regions.

Nsp13 functions as a unified ATP-independent nucleic acid remodeler across diverse substrates

Based on the comprehensive characterization of Nsp13's ATP-independent unwinding activities on duplex DNA, RNA, and G4 (Figures 2-5), we further investigated whether it possesses broader nucleic acid remodeling functions[9].

Nsp13 demonstrated potent strand-annealing activity. It efficiently facilitated the hybridization of complementary single-stranded DNA into various duplex structures-including those with 5'-overhang, 3'-overhang, and fork-without any requirement for ATP (Figure 6A-C; Figure S11A-D). Systematic analysis across multiple DNA substrates revealed a consistent biphasic dependence of annealing efficiency on Nsp13 concentration, particularly evident in the presence of Mg^{2+} alone. The activity increased sharply at low nanomolar concentrations, reached an optimum at approximately 200 nM, and then declined significantly with further increases in protein concentration (Figure 6B, S11A-D). This non-monotonic pattern suggests a self-regulatory mechanism, potentially arising from non-productive substrate sequestration or protein oligomerization at elevated concentrations. Crucially, the simultaneous presence of ATP and Mg^{2+} switched Nsp13's function from annealing to rapid unwinding, highlighting its dynamic operational mode (Figure 6B-C).

In parallel, Nsp13 exhibited RNA strand-annealing activity with distinct substrate specificity and cofactor sensitivity. In the absence of both Mg^{2+} and ATP, Nsp13 efficiently promoted annealing of RNA substrates with 5'-overhang and fork structures, while showing minimal activity on 3'-

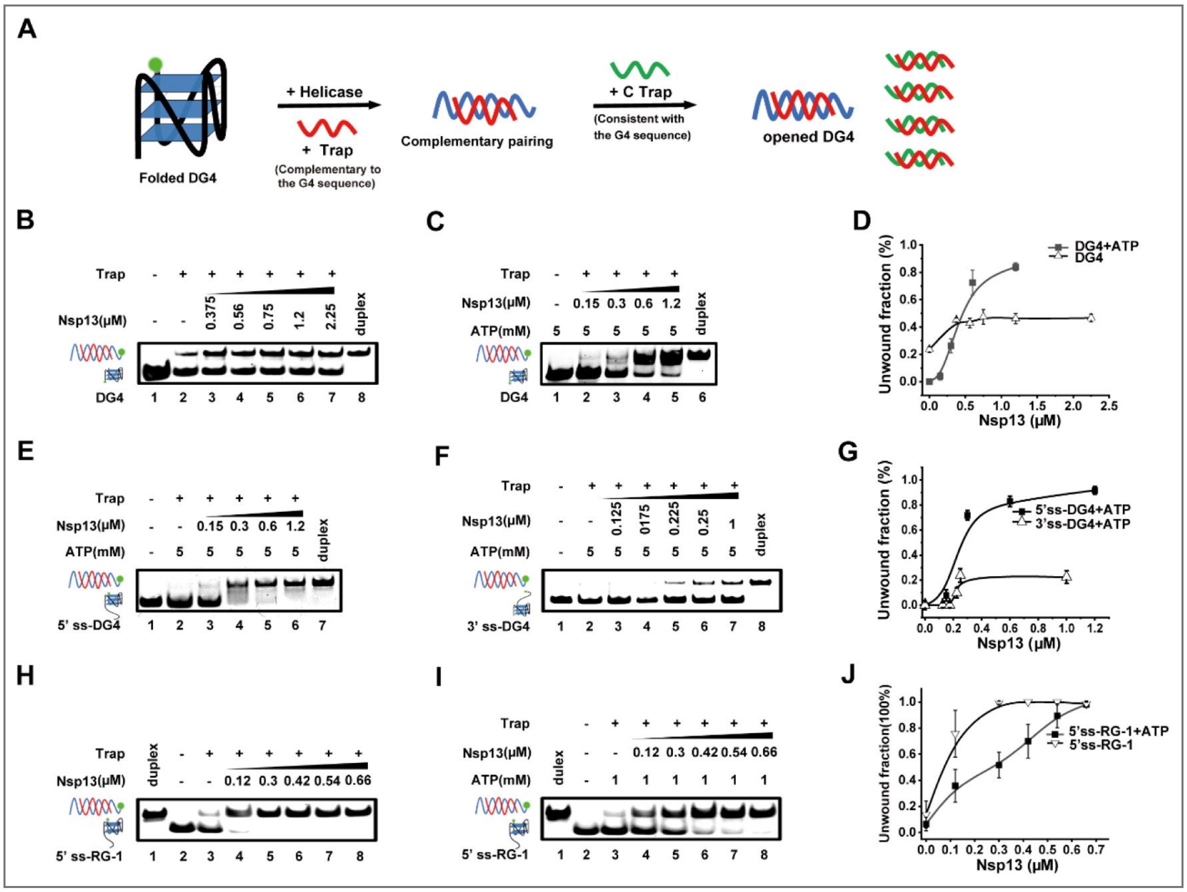

Figure 5. **Nsp13 unwinds G4 structures through dual ATP-dependent and -independent pathways.**

(A) Schematic of the G4 unfolding assay. (B–C) EMSA showing ATP-independent and ATP-dependent unfolding of blunt-ended DG4 (30 nM). (D) Quantification of DG4 unfolding efficiency. (E–F) EMSA showing direction-dependent unwinding of 5'- and 3'-overhang DG4 (25 nM) substrates. (G) Quantification confirming 5'→3' directionality. (H–I) EMSA showing ATP-independent and ATP-dependent unfolding of SARS-CoV-2 RNA G4 (RG-1, 60 nM). (J) Quantification of RG-1 unfolding efficiency.

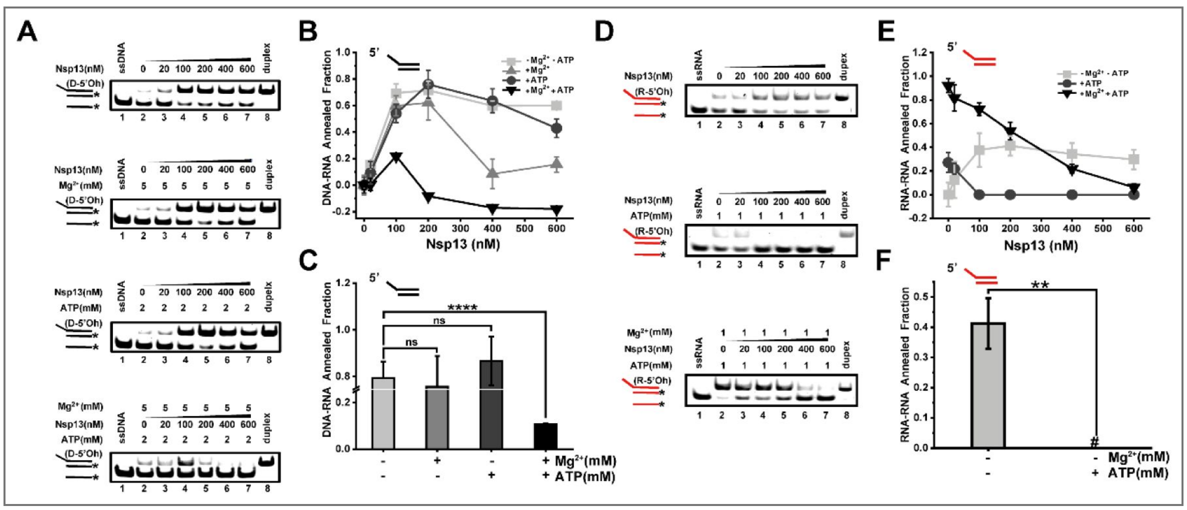

Figure 6. **Nsp13 exhibits ATP/Mg^{2+}-independent nucleic acid annealing activity.**

(A) EMSA of DNA strand annealing by Nsp13 under four cofactor conditions: no Mg^{2+}/ATP, Mg^{2+} only, ATP only, and Mg^{2+}+ATP. (B) Concentration-response curve showing biphasic DNA annealing. (C) Quantification of DNA annealing efficiency at 200 nM Nsp13. (D) EMSA of RNA strand annealing under three cofactor conditions: no Mg^{2+}/ATP, ATP only, and Mg^{2+}+ATP. The Mg^{2+}-only condition was omitted because 1 mM Mg^{2+} promotes spontaneous hybridization of the single-stranded RNA substrates. (E) Concentration-response curve of RNA annealing. (F) Quantification of RNA annealing efficiency at 200 nM Nsp13. Data are presented as mean ± SD (n=3).

overhang or blunt ends (Figure S11E-G). The introduction of 1 mM ATP alone significantly suppressed this annealing activity (Figure 6D-F). Notably, in the presence of 1 mM Mg^{2+}, where substantial spontaneous RNA duplex formation occurred, the addition of 1 mM ATP triggered a functional switch from annealing to robust unwinding (Figure 6D-E). This cofactor-dependent transition reveals a finely tuned dynamic equilibrium that is uniquely adapted for RNA substrate remodeling.

To further examine its chaperone function, we employed a classic strand-exchange assay[35] (Figure S12A). When incubated with Nsp13 in the absence of ATP, pre-folded DNA and RNA hairpins were efficiently destabilized, leading to a time-dependent formation of a more stable, hybridized duplex (Figure S12B-C). This remodeling was more efficient for DNA than RNA, consistent with the annealing results. The failure of a control 5'→3' helicase, ToPif1[36], to catalyze this reaction under identical conditions underscored the uniqueness of Nsp13's inherent chaperone activity (Figure S12D).

In conclusion, our work identifies a previously unreported fundamental aspect of SARS-CoV-2 Nsp13: a unified, ATP-independent nucleic acid remodeling function encompassing both strand annealing and secondary structure destabilization. This activity, operating alongside canonical ATP-dependent helicase function and modulated by cations, protein concentration, and substrate identity, provides the viral replication machinery with exceptional flexibility to manage complex nucleic acid structures throughout the viral life cycle.

Discussion

In this study, we redefine SARS-CoV-2 Nsp13 as a highly integrated, mode-switchable nucleic acid remodeler whose activity is dynamically regulated by cofactors, substrate architecture, and enzyme concentration. Rather than functioning solely as a canonical ATP-dependent helicase, Nsp13 coordinates motor-driven and ATP-independent remodeling activities within a single protein to manage structurally complex nucleic acids during viral replication and transcription.

Our results establish Nsp13 as an extreme example of functional integration within the helicase family, challenging the traditional view that helicase function is defined primarily by ATP-driven, unidirectional unwinding. In addition to its canonical helicase mode, Nsp13 destabilizes duplexes, hairpins, and G4s through a divalent cation–activated, ATP-independent pathway and catalyzes strand annealing and chaperone-like restructuring. These activities are not independent but are coordinated and selectively engaged by physicochemical cues such as Mg^{2+} availability, substrate topology, and protein concentration (Figure 7).

This integrated framework reconciles and extends prior observations on coronavirus helicases. SARS-CoV Nsp13 exhibits ADP-stimulated chaperone activity[24], and SARS-CoV-2 Nsp13 has been reported to resolve RNA stem-loops via ATP-independent mechanisms[25]. Our data provide a unifying mechanistic basis by showing that Mg^{2+} allosterically stabilizes compact RecA1–RecA2 configurations, enabling ATP-independent remodeling while modulating ATP-dependent motor activity. Nsp13 therefore functions not as a single-mode enzyme but as an integrated system whose catalytic output emerges from dynamic conformational regulation.

A key advance of this work is the identification of a robust ATP-independent remodeling mode activated by divalent cations. This activity does not result from nonspecific substrate destabilization, as Mg^{2+} alone stabilizes duplex DNA. Instead, structural modeling and thermal analyses indicate that Mg^{2+} acts as an allosteric effector that primes Nsp13 for low-processivity strand displacement. Preservation of this activity in ATPase-deficient mutants and its enhancement by non-hydrolyzable nucleotides support a hierarchical activation model in which metal-ion binding establishes a remodeling-competent state, while nucleotide binding fine-tunes activity levels. This ATP-independent mode has profound potential implications for the viral lifecycle. It could allow Nsp13 to remain functionally active in cellular niches with low ATP availability or to perform "quick" structural adjustments on nucleic acids without the energetic cost of ATP hydrolysis.

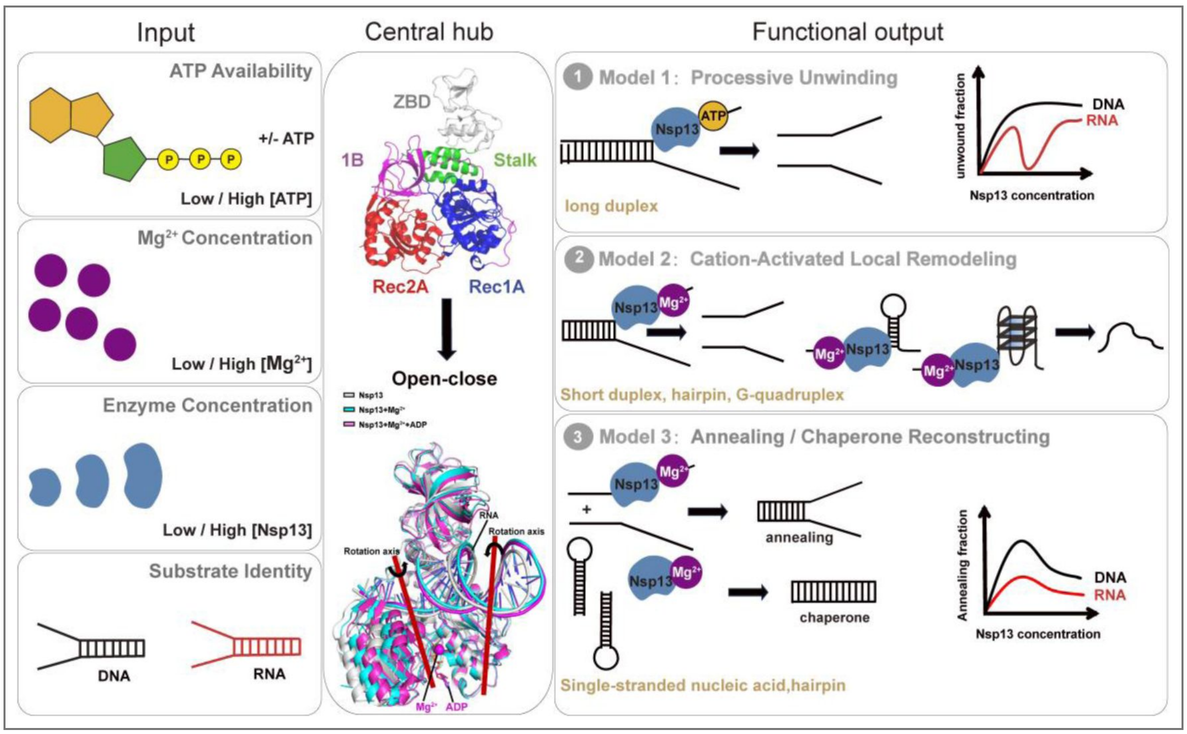

Figure 7. **An integrated functional model of Nsp13 as a tunable nucleic acid remodeler.**

Nsp13 integrates key inputs—cofactors (ATP/Mg^{2+}), enzyme concentration, and substrate topology—through a central regulatory hub where Mg^{2+} or Mg^{2+}-nucleotide complex allosterically stabilizes its compact RecA1–RecA2 conformation. This tunable hub drives three distinct functional outputs: (1) ATP-dependent processive unwinding, (2) Mg^{2+}-primed ATP-independent remodeling, and (3) ATP-independent strand annealing and chaperoning. The coordinated switching among these outputs enables Nsp13 to operate as a multifunctional, context-sensitive remodeler that supports diverse nucleic-acid transactions during viral replication and transcription.

Our findings further demonstrate that unwinding polarity and functional output of Nsp13 are not intrinsic constants but emergent properties shaped by substrate architecture and energetic context. Duplex DNA supports bidirectional remodeling via both ATP-dependent and ATP-independent mechanisms, consistent with cryo-EM observations of 3'→5' RNA unwinding within the replication–transcription complex[26]. In contrast, G4s show a strong 5'→3' bias, suggesting higher-order structures impose geometric constraints. RNA substrates additionally reveal pronounced Mg^{2+} sensitivity and nonlinear concentration dependence, highlighting the importance of substrate-specific regulatory logic in governing Nsp13 activity.

Together, these properties provide SARS-CoV-2 with a versatile mechanism to manage its large and structurally complex RNA genome. By integrating multiple remodeling activities, Nsp13 can both resolve obstructive secondary structures and G4s ahead of the replication fork and rescue misfolded RNA intermediates. Notably, the strand-annealing activity may play a key role during discontinuous transcription[37], potentially facilitating template switching essential for subgenomic RNA synthesis[38]. By consolidating these functions within a single protein, Nsp13 reduces reliance on multiple specialized host factors, thereby enhancing viral replication efficiency and autonomy. More broadly, our findings reveal that helicases can encode far greater functional versatility than implied by classical motor-centric definitions, highlighting new conceptual and therapeutic opportunities for targeting viral replication through noncanonical helicase mechanisms.

Materials and Methods

Nucleic acid substrates

DNA oligonucleotides were synthesized and HPLC-purified by Sangon Biotech; RNA oligonucleotides by Jinsirui Biotechnology. Sequences and modifications are listed in Table S1. DNA and RNA duplexes were prepared by annealing a FAM-labeled strand (2 μM) with 1.2-fold excess of complementary strand in 20 mM Tris-HCl pH 7.5, 50 mM NaCl, heating at 95°C for 10 min, and cooling to room temperature overnight. G4s were folded by heating 2 μM DNA or RNA in 20 mM Tris-HCl pH 7.5, 100 mM KCl, followed by slow cooling. Hairpins were heat-denatured at 95°C for 5 min and snap-cooled on ice.

Protein expression and purification

SARS-CoV-2 Nsp13 (GenBank: OR099200.1) was cloned into pET28a with an N-terminal His_6 tag. Plasmids were transformed into *E. coli* Rosetta (DE3) and grown at 37°C on a shaking incubator at 200 rpm for 3 hours until OD_{600} reached approximately 0.8. At this point, cultures were rapidly cooled in an ice-water bath and then incubated at 18°C for 20 hours for self-induction. Cells were lysed in 25 mM HEPES pH 7.0, 500 mM NaCl, 20% glycerol, 5 mM imidazole, 2 mM EDTA, 2 mM DTT. Lysates were applied to His-tag resin, washed with 800 mM NaCl, eluted with 250 mM imidazole, and further purified on a HiTrap Heparin column. Proteins were concentrated, aliquoted, and stored at −80°C. ATPase-deficient mutant K288R and a His-tag-free Nsp13 variant (generated by inserting a SUMO protease cleavage site between the His-tag and Nsp13) were purified using the same protocol.

LC-MS/MS analysis

Purified Nsp13 was digested with trypsin at 37°C for 12 h. Peptides were desalted, dissolved in 0.1% formic acid, and analyzed on a Fusion Lumos mass spectrometer with PepMap C18 trap (300 μm × 35 mm) and analytical column (75 μm × 150 mm). Data were processed with Proteome Discoverer 2.2 (FDR: 1% strict, 5% relaxed).

Nucleic acid binding assay

Fluorescence anisotropy was measured on an Infinite F200 (Tecan)[27]. Increasing concentrations of Nsp13 were titrated into 5 nM FAM-labeled nucleic acid in 25 mM Tris-HCl pH 7.5, 20 mM NaCl or KCl (for G4s), 2 mM DTT, and incubated at 37°C for 5 min. Data were fitted to the Hill equation to determine Kd and Hill coefficient (n).

ATPase activity assay

ATP hydrolysis was measured using the Malachite Green Phosphate Assay Kit (Sigma). Reactions (40 µL) contained 25 mM Tris-HCl pH 7.5, 20 mM NaCl, 5 mM $MgCl_2$, 2 mM DTT, 1 µM nucleic acid, 1 mM ATP, 400 nM Nsp13, incubated at 37°C for 5 min. Pi release was quantified at 620 nm.

Helicase unwinding assay

Unwinding reactions were performed by incubating Nsp13 with 40 nM dsDNA or dsRNA substrate in unwinding buffer (25 mM Tris-HCl pH 7.5, 20 mM NaCl, 2 mM DTT) at 37°C for 30 min. Reactions included 0–10 mM $MgCl_2$, 0–10 mM ATP, and a 20-fold molar excess of unlabeled trap strand (Table S1). DNA unwinding was stopped with 10 × stop buffer (50 mM Tris pH 7.5, 50% glycerol, 1% SDS, 0.1% bromophenol blue). RNA reactions were terminated with 10 × stop buffer (50 mM Tris pH 7.5, 50% glycerol, 2% SDS, 100 mM EDTA, 0.1% bromophenol blue) and digested with 20 mg/mL proteinase K. Products were resolved on 10% (DNA) or 15% (RNA) native PAGE gels, visualized with a ChemiDoc MP system (Bio-Rad), and quantified using ImageJ.

G4 unfolding assay

DG4 (25-30 nM) or RG-1 (60 nM) was incubated with Nsp13 in substrate-specific buffers (DG4: 25 mM Tris-HCl pH 7.5, 20 mM KCl, 5 mM Mg^{2+}; RG-1: 25 mM Tris-HCl pH 7.5, 20 mM KCl, 1 mM Mg^{2+}). Reactions were initiated with 1 mM ATP and 30–36 nM trap strand, incubated for 3 min, stopped with 10 × stop buffer (50 mM Tris pH 7.5, 50% glycerol, 1% SDS, 0.1% bromophenol blue), followed by addition of a 20-fold C-trap.

Nucleic acid annealing assay

Reactions contained 20 nM substrate and complementary strand in 25 mM Tris-HCl pH 7.5, 20 mM NaCl. Specific conditions included 5 mM Mg^{2+} for Mg^{2+}-dependent annealing, 2 mM ATP for ATP-dependent annealing, or 1 mM Mg^{2+} for RNA-specific annealing. Reactions were initiated by Nsp13 addition, stopped with 10 × stop buffer (100 mM EDTA, 2% SDS, 50% glycerol, 0.1% bromophenol blue) and 20-fold trap strand, resolved on 10% (DNA) or 15% (RNA) native PAGE.

Chaperone activity

Pre-folded hairpin DNA or RNA (20 nM each, one FAM-labeled) was incubated with 3 µM Nsp13 in 25 mM Tris-HCl pH 7.5, 20 mM NaCl, 2 mM DTT, 5 mM $MgCl_2$ (DNA) or 1 mM $MgCl_2$ (RNA) at 37°C for 1 h. Reactions were stopped with 10× stop buffer (50 mM Tris pH 7.5, 50% glycerol, 2% SDS, 100 mM EDTA, 0.1% bromophenol blue) and analyzed by native PAGE.

FRET melting

FAM/HEX-labeled duplex DNA (0.5 µM) was melted from 25°C to 95°C on a Rotor-Gene Q (Qiagen). FAM emission was normalized, and Tm was defined at 0.5 normalized emission.

Circular dichroism (CD) thermal denaturation

Protein stability was measured on a Jasco J-1500 spectropolarimeter. Nsp13 (3 µM) in unwinding buffer was heated from 25°C to 95°C at 2°C/min. CD spectra were recorded from 200–260 nm (1 nm bandwidth); melting curves at 222 nm were fitted to the Boltzmann equation to determine Tm.

Alphafold3 prediction

Structures of SARS-CoV-2 Nsp13 and its K288R variant were predicted using the AlphaFold3 server. Select predictions included Mg^{2+}, ATP (or analogs), and RNA duplexes or hairpins as ligands. Only predictions meeting the following quality criteria were analyzed: pLDDT > 90 for all ligand-coordinating residues, pTM ≥ 0.9, and ipTM ≥ 0.7.

Supplementary information

Name	Sequence (5' to 3')
	sequences for ATPase activity
ssRNA	UUUUUUUUUUCUCUGCUCGACG
	sequences for fluorescence anisotropy assay
ssDNA	CACTGGCCGTCTTACGGTCGCTCTGCTCGACG-FAM
ssRNA	UUUUUUUUUUCUCUGCUCGACG-FAM
5’ss-RG4	FAM-UUUUUUUUUUUUUGGGUUAGGGUUAGGGUUAGGG
3’ss-RG4	FAM-GGGUUAGGGUUAGGGUUAGGGUUUUUUUUUUUUU
RG4	FAM-GGGUUAGGGUUAGGGUUAGGG
5’ss-R-HP	FAM-UUUUUUUUUUUUUUUCUCUGCUCGACGUUUUUUCGUCGAGCAGAG
3’ss-R-HP	FAM-UCUCUGCUCGACGUUUUUUCGUCGAGCAGAGUUUUUUUUUUUUUU
5’ss-DG4	TTTTTTTTTTGGGTTAGGGTTAGGGTTAGGG-FAM
3’ss-DG4	FAM-GGGUUAGGGUUAGGGUUAGGGUUUUUUUUUUUUU
DG4	FAM-TGGGTTAGGGTTAGGGTTAGGG
	sequences for unwinding assay
5’Oh$_{S14D16}$	TTTTTTTTTTTTTTCGCTGATGTCGCCTGG FAM-CCAGGCGACATCAGCG
5’Oh$_{S14D16}$-Trap	CCAGGCGACATCAGCG
3’Oh$_{D16S14}$	AATCCGTCGAGCAGAGTTTTTTTTTTTTTT CTCTGCTCGACGGATT-FAM
3’Oh$_{D16S14}$-Trap	CTCTGCTCGACGGATT
3’Oh$_{D12S12}$	CGCTGATGTCGCTTTTTTTTTTTTTT GCGACATCAGCG-FAM
3’Oh$_{D12S12}$-Trap	GCGACATCAGCG
RNA-fork	UUUUUUUUUUCUCUGCUCUAUG-FAM CAUAGAGCAGAGUUUUUUUUUU
RNA-fork-Trap	CTCTGCTCTATG
5’Oh$_{S14D24}$	TTTTTTTTTTTTTTGCTCTGGTGCCGACCAACGAGAGT FAM-ACTCTCGTTGGTCGGCACCAGAGC
5’Oh$_{S14D24}$ -Trap	ACTCTCGTTGGTCGGCACCAGAGC
DG4 Trap	GCAGAGATCCCTAACCCTAACCCTAACCCTTTTTTTT
C trap	GGGTTAGGGTTAGGGTTAGGG
5’ss-RG-1	UUUUUUUUUUGGCUGGCAAUGGCGGU-FAM
RG-1-Trap	GCAGAGATCCGCCATTGCCAGCCTTTTTTTT
RG-1-C-Trap	GGCTGGCAATGGCGG
	sequences for annealing assay
D-Y	TTTTTTTTTTTTTTGCTCTGGTGCCGACCAACGAGAGT FAM-ACTCTCGTTGGTCGGCACCAGAGCTTTTTTTTTTTTTT
D-3’Oh	GCTCTGGTGCCGACCAACGAGAGTTTTTTTTTTTTTTT FAM-ACTCTCGTTGGTCGGCACCAGAGC
D-5’Oh	TTTTTTTTTTTTTTGCTCTGGTGCCGACCAACGAGAGT FAM-ACTCTCGTTGGTCGGCACCAGAGC
D-blunt	FAM-ACTCTCGTTGGTCGGCACCAGAGC GCTCTGGTGCCGACCAACGAGAGT
R-3’Oh	CGUCGAGCAGAGUUUUUUUUUUUU CUCUGCUCGACG-FAM
R-5’Oh	UUUUUUUUUUUUCGUCGAGCAGAG CUCUGCUCGACG-FAM
R-Y	UUUUUUUUUUCUCUGCUCGACG-FAM CGUCGAGCAGAGUUUUUUUUUUUU
R-blunt	CUCUGCUCGACG-FAM CGUCGAGCAGAG
Trap-DNA annealing	ACTCTCGTTGGTCGGCACCAGAGC

Trap-RNA annealing	CTCTGCTCGACG
	sequences for chaperone assay
D-chaperone	GATTATCCGATAGTCGAAGCTAGGTTCCACTATCCGATAATG **FAM**-CATTATCGGATAGTGGAACCTAGCTTCGACTATCGGATAATC
R-chaperone	GAUUAUCCGAUAGUCGAAGCUAGGUUCCACUAUCCGAUAAUG **FAM**-CAUUAUCGGAUAUGGGAACCUAGCUUCGACUAUCGGAUAAUC
	sequences for FRET melting assay
5’Oh$_{S14D16}$	TTTTTTTTTTTTTTCGCTGATGTCGCCTGG-**FAM** **HF**-CCAGGCGACATCAGCG

Note: FAM, fluorescein; HF, hexachlorofluorescein.

Table S1. **DNA and RNA sequences used in different assays.**

Table S2. **SARS-CoV-2 Nsp13 mass spectrometry.**

prot_num	prot_acc	prot_cove（%）	MW（kDa）	pep_count
1	SARS-CoV-2 NSP13	87	66.9	72
2	A1A766	10	69.1	5
3	A1AIF3	8	43.3	3
4	P0CD71	9	43.3	3
5	P0AEX9	8	43.4	3
6	P0AA25	31	11.8	2
7	P41168	4	50.6	2
8	P11221	25	8.8	2
9	P0A6F5	6	57.3	2

Note: The second column is the NCBI protein accession number.

Table S3. **Binding parameter of SARS-CoV-2 Nsp13.**

	Binding parameters	
Substrate	***Kd*(nM)**	***n***
ssDNA	15.83±1.26	1.3
ssRNA	19.85±0.90	2.0
5’ss-RG4	11.60±0.79	1.6
3’ss-RG4	13.1±0.81	2.3
RG4	20.4±3.94	0.9
5’ss-R-HP	10.85±0.43	2.7
3’ss-R-HP	33.02±0.40	1.1
5’ss-DG4	21.3±0.70	1.3
3’ss-DG4	26.0±0.58	2.3
DG4	51.6±3.56	1.6

Figure S1. **Binding affinity of Nsp13 to various nucleic acid substrates measured by fluorescence anisotropy.**

Binding isotherms of Nsp13 to (A) single-stranded DNA (ssDNA) and single-stranded RNA (ssRNA); (B) RNA hairpin; (C) DNA G-quadruplex (DG4); and (D) RNA G-quadruplex (RG4). Data are presented as mean ± SD from three independent experiments. Curves were fitted to the Hill equation to determine the equilibrium dissociation constant (*K*d) and Hill coefficient (n).

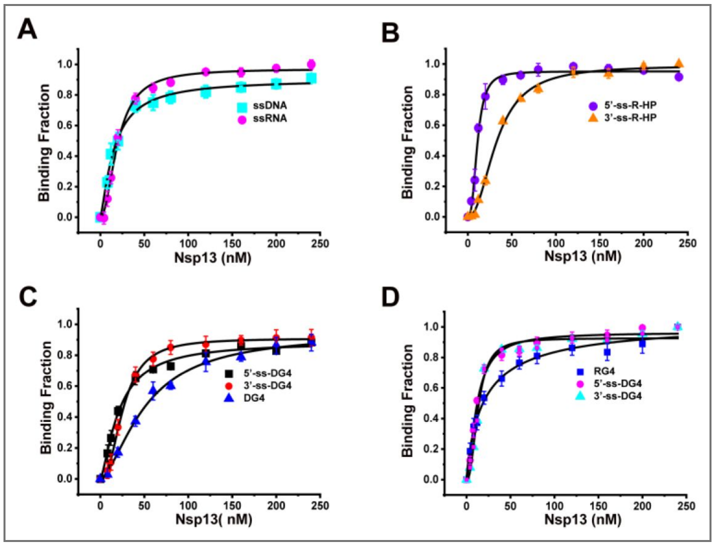

Figure S2. **Verification of ATP-independent DNA unwinding by His-tag-free Nsp13.**

(A) EMSA showing ATP-independent DNA unwinding by His-tag-free Nsp13 (Nsp13-notag). (B) Quantification of unwound DNA fraction illustrating the effect of Mg^{2+} concentration on ATP-independent unwinding. Data are presented as mean ± SD (n=3). Statistical significance was determined by unpaired Student's t-test.

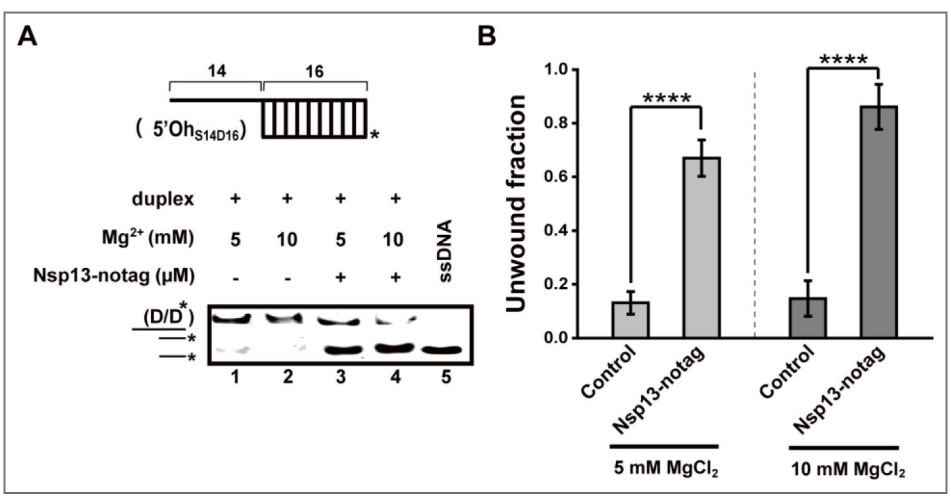

Figure S3. Mechanism of Mg^{2+}-mediated DNA unwinding by Nsp13.

(A)FRET-melting curves of duplex DNA in the presence of increasing Mg^{2+} concentrations (0–8 mM). (B) FRET-melting curves of duplex DNA in the presence of increasing Nsp13 concentrations (0–1.8 μM). (C) Bar graph showing that Nsp13 does not destabilize the duplex DNA substrate. (D) Binding curves of Nsp13 to duplex DNA in the presence of 0 mM and 0.5 mM Mg^{2+}.

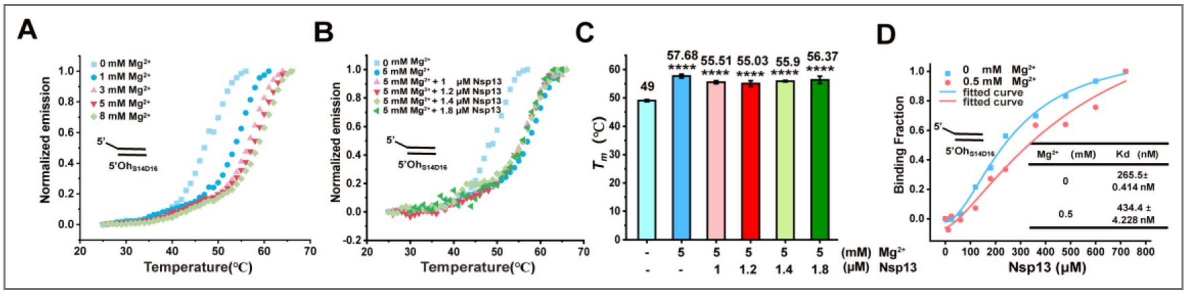

Figure S4. AlphaFold3-predicted Nsp13.

(A) The predicted structure of apo Nsp13 aligns well with the experimental structure 7nio from the PDB. (B) Nsp13-ss/dsRNA complex with Mg^{2+} and ADP. Mg^{2+} binds in the RecA1–RecA2 cleft and induces structural compaction. ADP binding further stabilizes the closed conformation.

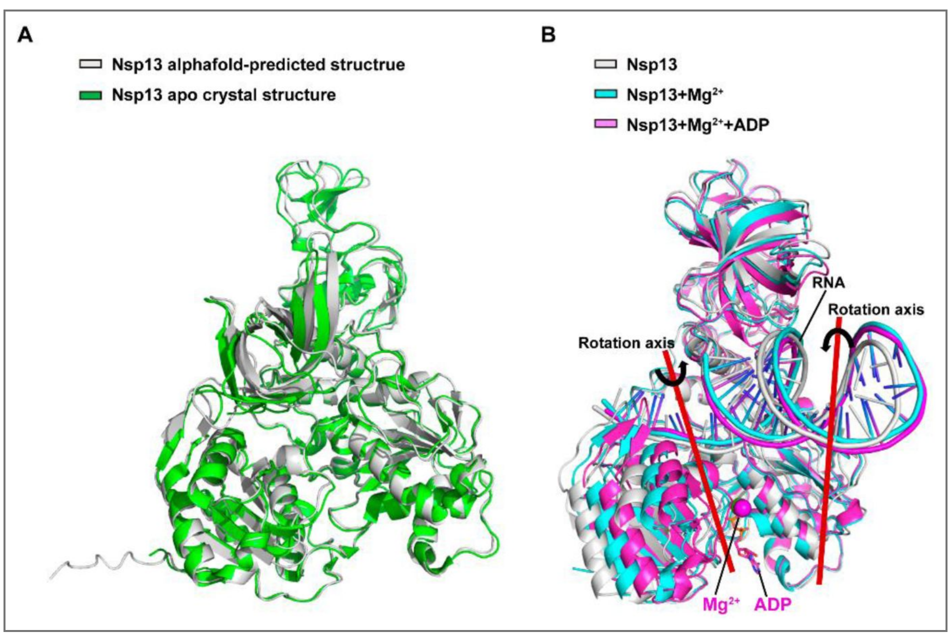

Figure S5. AlphaFold3-predicted structures of Nsp13-ATP-Mg^{2+} and K288R-ATP-Mg^{2+} complexes.

Cartoon representation: Nsp13-ATP-Mg^{2+} in green, K288R-ATP-Mg^{2+} in orange. ATP molecules are shown as sticks, and Mg^{2+} ions as purple spheres.

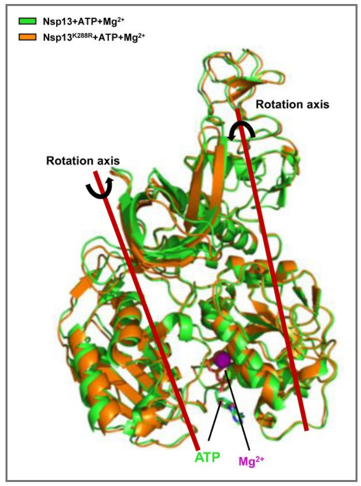

Figure S6. The ATP/Mg^{2+} ratio fine-tunes Nsp13 unwinding of duplex DNA and Nsp13 exhibits 3'→5' unwinding activity.

(A) EMSA (left) and quantification (right) demonstrating that increasing Mg^{2+} concentrations inhibit Nsp13-mediated unwinding at a fixed ATP level (1 mM). The 5'-overhang substrate 5'Oh$_{S14D24}$ (40 nM) was used. (B) Balanced ATP/Mg^{2+} sustains unwinding efficiency. EMSA (left) and quantification (right) showing that maintaining a 1:1 stoichiometry between ATP and Mg^{2+} preserves robust unwinding across a range of ATP concentrations (1–5 mM). All data represent mean ± SD from three independent experiments. (C) Schematic of the 3'-overhang DNA substrate (3'Oh$_{D16S14}$). EMSA illustrates efficient unwinding by Nsp13 in the presence of 5–10 mM Mg^{2+}, either without or with 2 mM ATP. Note: The FAM-labeled ssDNA strand migrates more slowly than the enzyme-released unwound product, likely due to secondary structure formation in the absence of Nsp13.

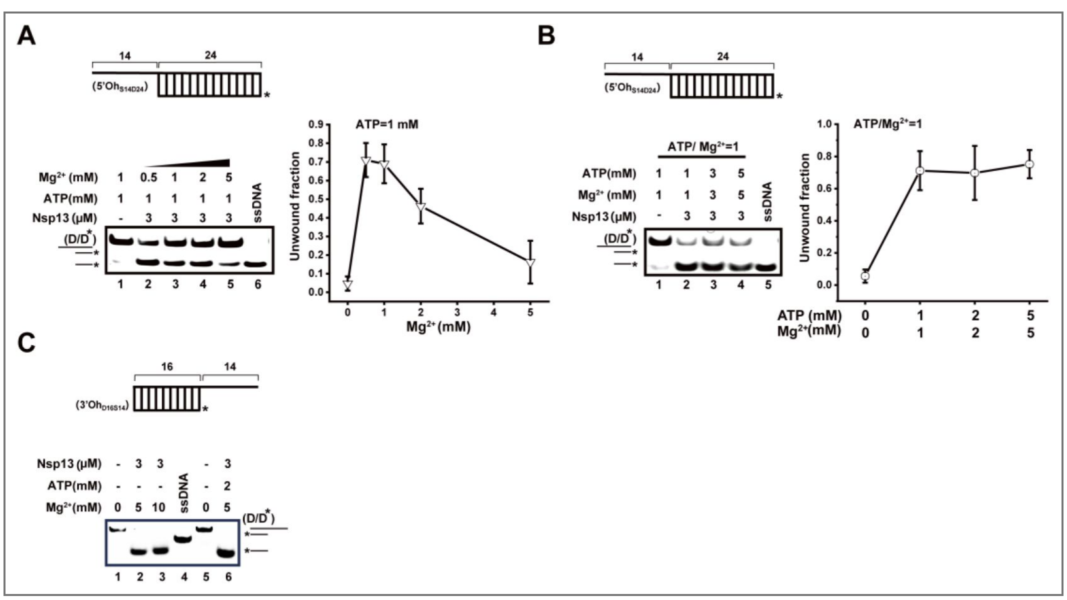

Figure S7. **Mg^{2+} and Nsp13 concentration dependence of RNA fork unwinding.**

(A) EMSA showing RNA unwinding by Nsp13 in the absence of ATP at 0 mM and 1 mM Mg^{2+}. (B) EMSA analysis of RNA unwinding by the ATPase-deficient mutant K288R at low Nsp13 concentration (80 nM) under different ATP conditions. (C) Quantification of unwound RNA fractions at 0.5 mM Mg^{2+} as a function of Nsp13 concentration, reproduced from Figure 4A. Data represent mean ± SD from three independent replicates.

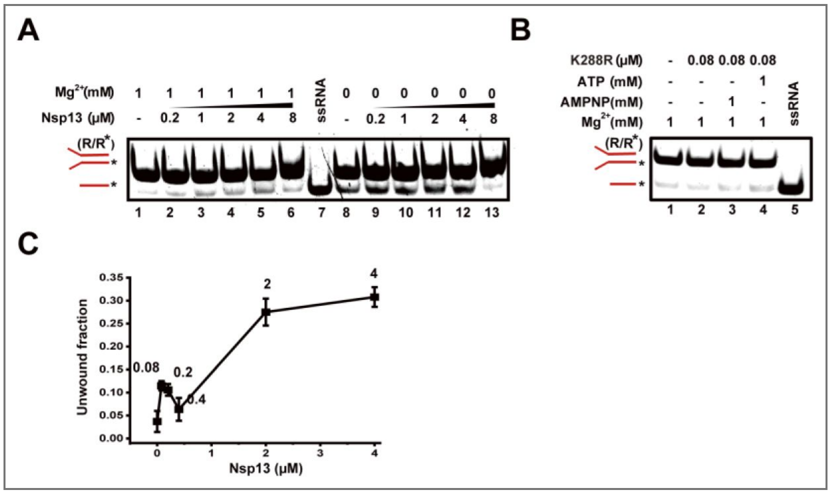

Figure S8. **Analysis of RNA duplex unwinding under inhibitory Nsp13 conditions.**

EMSA showing RNA duplex unwinding at the same Nsp13 concentration (0.4 μM) that inhibited RNA unwinding in Figure 4H in the presence of 1 mM ATP–Mg^{2+}, but using a different RNA substrate concentration (40 nM vs. 80 nM).

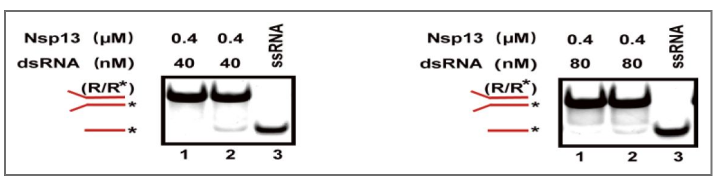

Figure S9. **ATP-dependent DNA unwinding by Nsp13 increases with protein concentration.**

(A) EMSA analysis of helicase activity on duplex DNA with increasing Nsp13 concentrations (0.02–3.2 μM). Reaction conditions: 40 nM DNA, 1 mM Mg^{2+}, 1 mM ATP, 37°C. (B) Quantification of unwound DNA fractions. Data represent mean ± SD from three replicates.

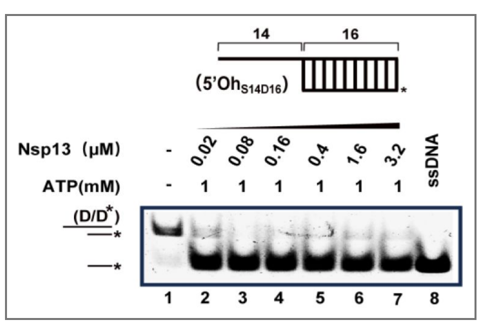

Figure S10. **EMSA analysis of SARS-CoV-2 RNA G-quadruplex (RG-1) unfolding by varying concentrations of Nsp13 in 1 mM Mg^{2+}.**

Partial unfolding was observed at low to moderate protein concentrations, whereas higher Nsp13 levels inhibited G4 unfolding.

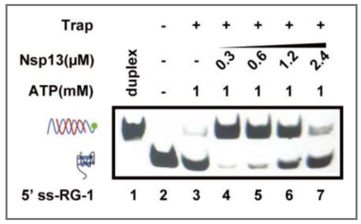

Figure S11. **Nsp13 exhibits ATP- and Mg^{2+}-independent strand annealing activity on diverse DNA and RNA substrates.**

(A) Schematic of DNA and RNA substrate structures used in annealing assays. (B) EMSA results showing Nsp13-mediated annealing of DNA substrates with 5'-overhang, 3'-overhang, and fork structures, respectively. (C) Concentration–response curve of DNA annealing activity in the absence of Mg^{2+} and ATP. (D) Annealing efficiency for three DNA configurations at 200 nM Nsp13. (E) EMSA results showing RNA annealing with 5'-overhang, 3'-overhang, fork, and blunt-end substrates. (F) Concentration–response curve of RNA annealing activity in the absence of Mg^{2+} and ATP. (G) Annealing efficiency for four RNA configurations at 200 nM Nsp13. Data are presented as mean ± SD (n=3). Statistical significance was determined by one-way ANOVA with Tukey's HSD test; ***P < 0.001; ns, not significant. Note: DNA blunt-end substrates were excluded from the analysis due to instability under the annealing buffer conditions.

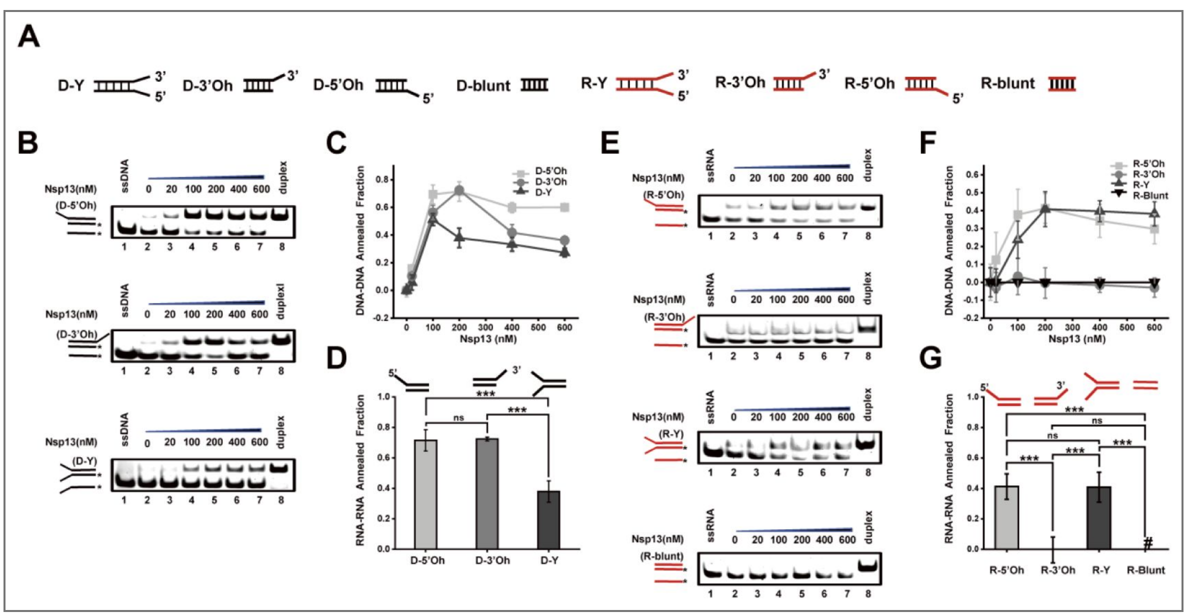

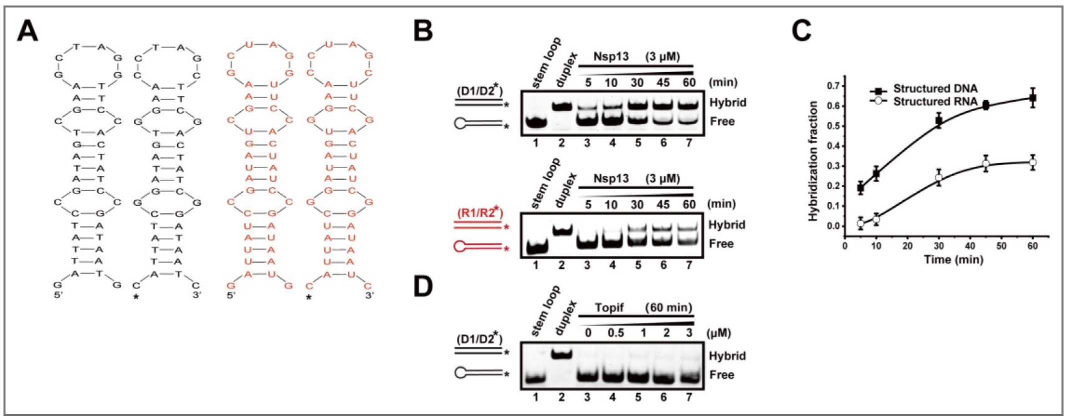

Figure S12. **Chaperone activity of Nsp13.**

(A) Schematic of the strand-exchange assay. Complementary 42-nt DNA and RNA stem-loops were used as substrates, with the FAM-labeled strands indicated by asterisks. (B–C) Time-course EMSA (B) and quantification (C) showing Nsp13-mediated strand exchange in the absence of ATP, demonstrating its intrinsic chaperone activity. Hybridization fraction was calculated from three independent replicates (mean ± SD). (D) Control experiment with ToPif1, a canonical 5'→3' helicase. Pre-folded DNA stem-loops were incubated with increasing concentrations of ToPif1 (0–3 μM) under identical conditions. No strand exchange was observed, confirming that the chaperone activity is unique to Nsp13 and not a general property of helicases. All reactions were performed with 20 nM FAM-labeled and unlabeled strands.

Data availability

All data presented in this study are available upon request.

Additional information

Funding

This work was supported by the National Natural Science Foundation of China (Grant No. 32571440) and the Frontier Interdisciplinary Innovation Project of the Future Agriculture Research Institute, Northwest A&F University (A1080525005).

Author contributions

Xi-Miao Hou: Conceptualization, Supervision, Writing- Reviewing and Editing. Hai-Hong Li: Investigation, Data curation, Writing- Original draft preparation. Jia-Li Hou, Xue-Yang Yu, Jie Jin: Investigation.

Funding

Funder	Grant reference number	Author
MOST | National Natural Science Foundation of China (NSFC)	32571440	Xi-Miao Hou

Author ORCID iDs

Xi-Miao Hou: https://orcid.org/0000-0003-3499-443X

References

[1] **Kim D.**, et al. (2020) The Architecture of SARS-CoV-2 Transcriptome. *Cell* **181**:914-921.e10

[2] **Huston N.C.**, et al. (2021) Comprehensive in vivo secondary structure of the SARS-CoV-2 genome reveals novel regulatory motifs and mechanisms. *Molecular cell* **81**:584-598.e5

[3] **Ji D.**, et al. (2021) Discovery of G-quadruplex-forming sequences in SARS-CoV-2. *Briefings in bioinformatics* **22**:1150-1160

[4] **Zhai L.**, et al. (2022) Recent advances in applying G-quadruplex for SARS-CoV-2 targeting and diagnosis: A review. *International journal of biological macromolecules* **221**:1476-1490

[5] **Zhai L.**, et al. (2022) Targeting the RNA G-Quadruplex and Protein Interactome for Antiviral Therapy. *Journal of medicinal chemistry* **65**:10161-10182

[6] **Zhao C.**, et al. (2021) Targeting RNA G-Quadruplex in SARS-CoV-2: A Promising Therapeutic Target for COVID-19?. *Angew Chem Int Ed Engl* **60**:432-438

[7] **Chauhan S.**, Woodson S.A. (2008) Tertiary interactions determine the accuracy of RNA folding. *Journal of the American Chemical Society* **130**:1296-1303

[8] **Musier-Forsyth K** (2010) RNA remodeling by chaperones and helicases. *RNA biology* **7**:632-633

[9] **Jarmoskaite I.**, Russell R. (2014) RNA helicase proteins as chaperones and remodelers. *Annual review of biochemistry* **83**:697-725

[10] **Yang J.**, et al. (2015) RNA chaperones encoded by RNA viruses. *Virologica Sinica* **30**:401-409

[11] **Bai C.**, Zhong Q., Gao G.F. (2022) Overview of SARS-CoV-2 genome-encoded proteins. *Science China Life sciences* **65**:280-294

[12] **Chen J.**, et al. (2020) Structural Basis for Helicase-Polymerase Coupling in the SARS-CoV-2 Replication-Transcription Complex. *Cell* **182**:1560-1573.e13

[13] **Shu T.,** et al. (2020) SARS-Coronavirus-2 Nsp13 Possesses NTPase and RNA Helicase Activities That Can Be Inhibited by Bismuth Salts. *Virologica Sinica* **35**:321-329

[14] **Tanner J.A.,** et al. (2003) The severe acute respiratory syndrome (SARS) coronavirus NTPase/helicase belongs to a distinct class of 5′ to 3′ viral helicases. *The Journal of biological chemistry* **278**:39578-39582

[15] **Jia Z.,** et al. (2019) Delicate structural coordination of the Severe Acute Respiratory Syndrome coronavirus Nsp13 upon ATP hydrolysis. *Nucleic acids research* **47**:6538-6550

[16] **Cao C.,** et al. (2021) Molecular epidemiology analysis of early variants of SARS-CoV-2 reveals the potential impact of mutations P504L and Y541C (NSP13) in the clinical COVID-19 outcomes. *Infection, genetics and evolution : journal of molecular epidemiology and evolutionary genetics in infectious diseases* **92**:104831-104831

[17] **Grimes S.L.,** Denison M.R. (2024) The Coronavirus helicase in replication. *Virus research* **346**:199401-199401

[18] **White M.A.,** Lin W., Cheng X. (2020) Discovery of COVID-19 Inhibitors Targeting the SARS-CoV-2 Nsp13 Helicase. *The journal of physical chemistry letters* **11**:9144-9151

[19] **Ugurel O.M.,** et al. (2020) Evaluation of the potency of FDA-approved drugs on wild type and mutant SARS-CoV-2 helicase (Nsp13). *International journal of biological macromolecules* **163**:1687-1696

[20] **Perez-Lemus G.R.,** et al. (2022) Toward wide-spectrum antivirals against coronaviruses: Molecular characterization of SARS-CoV-2 NSP13 helicase inhibitors. *Science advances* **8**:eabj4526-eabj4526

[21] **Marx S.K.,** et al. (2023) Observing inhibition of the SARS-CoV-2 helicase at single-nucleotide resolution. *Nucleic acids research* **51**:9266-9278

[22] **Sommers J.A.,** et al. (2023) Biochemical analysis of SARS-CoV-2 Nsp13 helicase implicated in COVID-19 and factors that regulate its catalytic functions. *The Journal of biological chemistry* **299**:102980-102980

[23] **Park J.,** et al. (2025) ATPase-dependent duplex nucleic acid unwinding by SARS-CoV-2 nsP13 relies on facile binding and translocation along single-stranded nucleic acid. *The Journal of biological chemistry* **301**:110373-110373

[24] **Yu J.,** et al. (2025) A novel ADP-directed chaperone function facilitates the ATP-driven motor activity of SARS-CoV helicase. *Nucleic acids research* **53**:gkaf034

[25] **Dumm A.J.,** et al. (2025) SARS-CoV-2 point mutations are over-represented in terminal loops of RNA stem-loop structures that can be resolved by Nsp13 helicase in a unique manner with respect to nucleotide dependence. *Nucleic acids research* **53**:gkaf447

[26] **Yan L.,** et al. (2025) Structural basis for the concurrence of template recycling and RNA capping in SARS-CoV-2. *Cell* **188**:7194-7205.e10

[27] **Dou S.,** Xi X.G. (2010) Fluorometric assays for characterizing DNA helicases. *Methods* **51**:295-302

[28] **Newman J.A.,** et al. (2021) Structure, mechanism and crystallographic fragment screening of the SARS-CoV-2 NSP13 helicase. *Nature communications* **12**:4848-4848

[29] **Maio N.,** et al. (2023) An iron-sulfur cluster in the zinc-binding domain of the SARS-CoV-2 helicase modulates its RNA-binding and -unwinding activities. *Proceedings of the National Academy of Sciences of the United States of America* **120**:e2303860120-e2303860120

[30] **Jang K.,** et al. (2020) A high ATP concentration enhances the cooperative translocation of the SARS coronavirus helicase nsP13 in the unwinding of duplex RNA. *Scientific reports* **10**:4481-4481

[31] **Liu G.,** et al. (2022) RNA G-quadruplex in TMPRSS2 reduces SARS-CoV-2 infection. *Nature communications* **13**:1444-1444

[32] **Qin G.,** et al. (2022) RNA G-quadruplex formed in SARS-CoV-2 used for COVID-19 treatment in animal models. *Cell discovery* **8**:86-86

[33] **Hou X.,** et al. (2017) Involvement of G-triplex and G-hairpin in the multi-pathway folding of human telomeric G-quadruplex. *Nucleic acids research* **45**:11401-11412

[34] **Miclot T.**, et al. (2021) Structure and Dynamics of RNA Guanine Quadruplexes in SARS-CoV-2 Genome. Original Strategies against Emerging Viruses. *The journal of physical chemistry letters* **12**:10277-10283

[35] **Yang J.**, et al. (2014) A cypovirus VP5 displays the RNA chaperone-like activity that destabilizes RNA helices and accelerates strand annealing. *Nucleic acids research* **42**:2538-2554

[36] **Dai Y.**, et al. (2022) Structural mechanism underpinning Thermus oshimai Pif1-mediated G-quadruplex unfolding. *EMBO reports* **23**:e53874-e53874

[37] **Wang D.**, et al. (2021) The SARS-CoV-2 subgenome landscape and its novel regulatory features. *Molecular cell* **81**:2135-2147.e5

[38] **Kim D.**, et al. (2020) The Architecture of SARS-CoV-2 Transcriptome. *Cell* **181**:914-921.e10

Peer reviews

Reviewer #1 (Public review):

In the manuscript by Li et al., the authors perform a comprehensive study on the template and cofactor determinants of the SARS-CoV-2 nsp13 protein. They find that, alongside the classical processive unwinding ability of helicases driven by ATP consumption, other chaperone-like and ATP-independent functions exist for this enzyme. By testing DNA and RNA oligos in several conformations, the authors show that these functions are highly dependent on template identity, but also on the ratio of ATP to divalent cations. Ultimately, it is suggested that these distinct mechanisms of action are employed by nsp13 to orchestrate viral replication.

Overall, this study provides some novel insights into the functionality of a central and conserved enzyme of a relevant human pathogenic virus. While the approach is important and adds to the field, particularly by characterizing the chaperoning activities and adding G-quadruplexes as templates, previous studies have already identified several determinants of nsp13 template binding and processing in vitro (Sommers et al., 2023, JBC; Park et al., 2025, JBC). In addition, some issues regarding experimental design need to be addressed to increase the cogency and biological relevance of the study.

(1) Generally, low concentrations of monovalent cations (20 mM), as used throughout this study, may influence helicase activity and artificially enhance protein binding/oligomerization, which could favor the observed chaperoning activity (Venus et al., 2022, Methods). In contrast, some helicases, such as HCV NS3, are inhibited by higher K^+ concentrations (Gwack et al., 2004, FEBS). Thus, the influence of higher concentrations of monovalent cations should be tested in relevant assays, as intracellular K^+ levels are usually >100 mM. Additionally, this could significantly affect template stability. For instance, in some G4 assays, the addition of the trap already leads to observable duplex formation (Figure 5), which may be due to low K^+ conditions.

(2) As in most publications that focus strictly on helicase (or other enzymatic) functions, the activity of the isolated protein is examined. However, particularly in the case of nsp13, core functions rely on other factors, such as nsp7/8 and other components of the replication-transcription complex (RTC). The overall structure and oligomerization state of nsp13 are altered within the complex (Chen et al., 2022, NSMB). The inclusion of such factors in key experiments would greatly improve the biological relevance of the findings.

(3) In Figure 4, the authors claim that Mg^{2+} concentration inhibits RNA unwinding. While this is likely considering previous findings, it must be validated that duplex stabilization is not the primary cause for the observed lower dissociation rates. As the template is only 12 bp long with extensive overhangs, higher ion concentrations may significantly stabilize base pairing

by reducing fraying effects. Similarly, in Figure 6, template-dependent effects of Mg2+/ATP should be ruled out.

(4) It is not entirely clear to me by which principle the templates were chosen. In my opinion, it would improve the overall comparability of the experimental results if, for instance, the blunt-ended duplex had the same sequence as the oligos with overhangs, since factors such as length, G/C content, Tm, etc., may play a significant role in binding and unwinding. Similarly, the oligos for binding and unwinding should be kept somewhat comparable, e.g., the G4 for the binding assay has 3 stacks, whereas RG1 has only 2. This discrepancy could make a significant difference. Thus, key experiments should be repeated using comparable sequence pairs.

Moreover, in the initial characterization of the binding abilities (Figure 1), the authors should include blunt-ended controls (duplex/hairpin) and, importantly, a pseudoknot (PK), as these structures are crucial for multiple steps in the viral life cycle (frameshifting, replication). Specifically, the PK in the 3'UTR (Sola et al., 2011, RNA Biology) may be an interesting target structure for unwinding assays, as it recruits the RTC, and, to my knowledge, no studies are available regarding nsp13 function at a PK. This would be particularly interesting in combination with nsp7/8 (Ohyama et al., 2024, JACS Au).

https://doi.org/10.7554/eLife.110731.1.sa2

Reviewer #2 (Public review):

Summary:

The authors are trying to broaden the understanding of SARS-CoV2 Nsp13 activity to show that a single viral protein can accomplish multiple functions. Additionally, they try to show that helicase function is not limited to ATP-driven, unidirectional unwinding.

Strengths:

The consistent application of statistics to triplicate experiments is a strength of the manuscript. The ToPif1 control in Figure S12 is a good control.

Weaknesses:

(1) All the experiments except the one in Figure S2 use N-terminally His-tagged Nsp13. Because the N-terminal tag is known to have large effects on Nsp13 activity, this calls into question virtually all of the results in this manuscript.

(2) The ATP-independent, bidirectional duplex unwinding shown for short duplex substrates is reminiscent of the trapping of thermal fraying intermediates that have been reported for other helicases. Because they are only observed on short duplexes, do not require ATP, and are bidirectional, this does not suggest strand displacement as suggested in the manuscript. Instead, it suggests trapping of partially melted intermediates.

(3) Results that may be artifacts of unusual in vitro conditions are interpreted as if similar results will occur in the cell, where ATP is likely always present. Along those same lines, SARS-CoV-2 replicates in compartments of the endoplasmic reticulum, which would limit the ability of Nsp13 to access DNA substrates.

(4) There is no evidence to support the conclusion that "Duplex DNA supports bidirectional remodeling via both ATP-dependent and ATP-independent mechanisms." 3'-5' duplex melting is limited to short duplexes and is ATP-independent, suggesting it may be due to trapping of thermal fraying intermediates by the ssDNA binding Nsp13. The ATP-dependent and ATP-independent melting on the substrates with the 3'-overhang are the same, suggesting that

ATP-dependent melting does not occur on this substrate, which would indicate that bidirectional ATP-dependent translocation does not occur.

(5) The description of ATP-independent unwinding as having "limited processivity," is likely not accurate. These experiments were multiturnover reactions with very high Nsp13 concentrations and no protein trap to ensure single turnover conditions. Because the reactions were multi-turnover, no information about the processivity of Nsp13 can be obtained. On the contrary, it seems likely that the product formed over the 30-minute reaction with a vast excess of Nsp13 is due to binding and dissociation of multiple Nsp13 molecules instead of processive translocation by a single enzyme.

(6) G4s are much more stable at cellular K+ concentrations than they are at 20 mM K+. As such, Nsp13's ability to unfold a G4 in the absence of ATP may be diminished or eliminated at a physiological K+ concentration.

Although the authors show that His-tagged Nsp13 can melt DNA and RNA duplexes and G-quadruplexes in an ATP-dependent and independent manner, in addition to annealing single-stranded nucleic acids into duplexes, the use of His-tagged Nsp13, which is known to cause artifacts, makes their results difficult to draw conclusions from. As such, in the opinion of this reviewer, this manuscript is likely to have little impact on the field.

https://doi.org/10.7554/eLife.110731.1.sa1

Author response:

> ***Public Reviews:***
>
> ***Reviewer #1 (Public review):***
>
> *In the manuscript by Li et al., the authors perform a comprehensive study on the template and cofactor determinants of the SARS-CoV-2 nsp13 protein. They find that, alongside the classical processive unwinding ability of helicases driven by ATP consumption, other chaperone-like and ATP-independent functions exist for this enzyme. By testing DNA and RNA oligos in several conformations, the authors show that these functions are highly dependent on template identity, but also on the ratio of ATP to divalent cations. Ultimately, it is suggested that these distinct mechanisms of action are employed by nsp13 to orchestrate viral replication.*
>
> *Overall, this study provides some novel insights into the functionality of a central and conserved enzyme of a relevant human pathogenic virus. While the approach is important and adds to the field, particularly by characterizing the chaperoning activities and adding G-quadruplexes as templates, previous studies have already identified several determinants of nsp13 template binding and processing in vitro (Sommers et al., 2023, JBC; Park et al., 2025, JBC). In addition, some issues regarding experimental design need to be addressed to increase the cogency and biological relevance of the study.*

We thank the reviewer for recognizing the novelty of our work, particularly the ATP-independent chaperone-like activities and G-quadruplex remodeling. We also appreciate the opportunity to clarify the conceptual distinction between our study and the prior work by Sommers et al. (2023) and Park et al. (2025). We fully agree that those studies systematically defined the canonical ATP-driven motor mechanism of Nsp13. Our results on 5'→3' polarity, DNA preference, and tail/ATP/Mg^{2+} dependence align with these benchmarks, confirming the reliability of our platform.

However, the core novelty of our work lies in revealing that Nsp13 functions as a multifaceted nucleic acid remodeler, integrating motor and non-motor activities within a single protein-a functional regime absent from the JBC papers. Specifically, we uncover three novel layers: 1. Mg^{2+}-activated, ATP-independent remodeling of short duplexes and G-quadruplexes. 2. Bidirectional remodeling on duplexes in the Mg^{2+}-primed state. 3. Intrinsic chaperone functions including strand annealing and stem-loop restructuring.

Thus, our work fundamentally expands the biochemical model of Nsp13 from a simple ATP-driven motor to a multifunctional, mode-switchable remodeler. We will highlight these distinctions in the revised Discussion. Below, we respond point-by-point to the specific experimental design issues.

> *(1) Generally, low concentrations of monovalent cations (20 mM), as used throughout this study, may influence helicase activity and artificially enhance protein binding/oligomerization, which could favor the observed chaperoning activity (Venus et al., 2022, Methods). In contrast, some helicases, such as HCV NS3, are inhibited by higher K+ concentrations (Gwack et al., 2004, FEBS). Thus, the influence of higher concentrations of monovalent cations should be tested in relevant assays, as intracellular K+ levels are usually >100 mM. Additionally, this could significantly affect template stability. For instance, in some G4 assays, the addition of the trap already leads to observable duplex formation (Figure 5), which may be due to low K+ conditions.*

We thank the reviewer for this critical comment regarding the ionic environment. We agree that monovalent cation concentrations are pivotal for both helicase activity and the structural stability of templates like G4s.

First, we wish to clarify that the final NaCl concentration in our reaction is not 20 mM, as this refers only to the unwinding buffer. Our protein dilution buffer contains 200 mM NaCl, and each 10 μL reaction includes 2 μL of protein, contributing ~40 mM NaCl. With 20 mM from the reaction buffer, the final concentration reaches~60 mM. We will clarify this in the Methods.

Second, our choice of ionic strength is guided by established literature. A survey of 27 published nsp13 studies (Author response table 1) shows that the majority use 20–50 mM monovalent cations, with 20 mM being most common. Mickolajczyk et al. (2021) showed that nsp13 activity is highest at low salt and declines at higher concentrations. Thus, low salt conditions are routinely used to capture nsp13's intrinsic catalytic activity. The intracellular environment is far more complex, with crowding and interacting proteins that likely modulate helicase behavior. The low-salt conditions are therefore a deliberate simplification to isolate and define enzyme function.

Planned experiments: We fully agree that higher salt concentrations should be tested. In the revision, we will perform key assays such as ATP-independent duplex unwinding and G4 unfolding at ≥100 mM NaCl or KCl to verify that the observed activities persist under more physiological ionic conditions

> *(2) As in most publications that focus strictly on helicase (or other enzymatic) functions, the activity of the isolated protein is examined. However, particularly in the case of nsp13, core functions rely on other factors, such as nsp7/8 and other components of the replication-transcription complex (RTC). The overall structure and oligomerization state of nsp13 are altered within the complex (Chen et al., 2022, NSMB). The inclusion of such factors in key experiments would greatly improve the biological relevance of the findings.*

We agree that examining Nsp13 within the context of the RTC is essential for establishing the biological relevance of our findings. The structural reorganization of Nsp13 upon binding to Nsp12 and Nsp7/8 (Chen et al., 2022) suggests that its enzymatic "mode" may be regulated by its protein partners.

Planned experiments: To address this, we will include the following biochemical characterizations:

(1) Nsp13/12 and Nsp13/7/8 sub-complexes will be examined to dissect the individual contributions of the polymerase and the primase-like factors to Nsp13's multifaceted activities.

(2) The core RTC (Nsp13/12/7/8) will be used to evaluate how the full assembly modulates the functions of Nsp13 particularly on complex templates like G4 and pseudoknots.

> *(3) In Figure 4, the authors claim that Mg2+ concentration inhibits RNA unwinding. While this is likely considering previous findings, it must be validated that duplex stabilization is not the primary cause for the observed lower dissociation rates. As the template is only 12 bp long with extensive overhangs, higher ion concentrations may significantly stabilize base pairing by reducing fraying effects. Similarly, in Figure 6, template-dependent effects of Mg2+/ATP should be ruled out.*

We thank the reviewer for this insightful suggestion. We agree that it is critical to distinguish whether the observed inhibition of RNA unwinding at higher Mg^{2+} concentrations is due to the physical stabilization of the RNA duplex.

Planned experiments: To address this, we will perform the following characterizations:

(1) We will measure the Tm of the RNA duplex used in Figure 4 across a range of Mg^{2+} concentrations (0, 0.5, and 1.0 mM). This will allow us to quantify the extent to which divalent cations stabilize the duplex RNA. These data will provide a more rigorous interpretation of the Mg^{2+}-dependent unwinding in Figure 4.

(2) Similarly, we will perform thermal melting analyses for the various DNA and RNA templates used in Figure 6 under different Mg^{2+}/ATP conditions to rule out the template-dependent effects of Mg^{2+}/ATP.

> *(4) It is not entirely clear to me by which principle the templates were chosen. In my opinion, it would improve the overall comparability of the experimental results if, for instance, the blunt-ended duplex had the same sequence as the oligos with overhangs, since factors such as length, G/C content, Tm, etc., may play a significant role in binding and unwinding. Similarly, the oligos for binding and unwinding should be kept somewhat comparable, e.g., the G4 for the binding assay has 3 stacks, whereas RG1 has only 2. This discrepancy could make a significant difference. Thus, key experiments should be repeated using comparable sequence pairs.*

We fully agree with the reviewer that maintaining sequence consistency across different assays is essential for a rigorous comparison of nsp13 activities. We apologize for the ambiguity in the initial presentation of our sequences in Table S1.

Planned revisions and experiments:

(1) We wish to clarify that several key substrates were sequence-matched. For unwinding assays, the 12-bp 3'-overhang DNA and blunt-ended DNA share the identical duplex sequence, and the 16-bp 5'-overhang and 3'-overhang DNA substrates are also sequence-matched. For annealing assays, the duplex regions for all DNA substrates (3', 5', blunt, and fork) are identical, and the same internal consistency was maintained for all RNA annealing substrates. To make this clear, we will reorganize Table S1 to explicitly group these sequence-paired substrates.

(2) The reviewer also notes discrepancies between binding and unwinding substrates (e.g., the difference in G4 stacks). To ensure direct comparability, we will perform additional experiments: complete binding assays for RG-1 (the 2-stack G4 used in unwinding) to match the functional data, and systematically measure binding affinities for all key unwinding substrates, including 3'-overhang, 5'-overhang, blunt-ended DNA, and the RNA fork.

> *(5) Moreover, in the initial characterization of the binding abilities (Figure 1), the authors should include blunt-ended controls (duplex/hairpin) and, importantly, a pseudoknot (PK), as these structures are crucial for multiple steps in the viral life cycle (frameshifting, replication). Specifically, the PK in the 3'UTR (Sola et al., 2011, RNA Biology) may be an interesting target structure for unwinding assays, as it recruits the RTC, and, to my knowledge, no studies are available regarding nsp13 function at a PK. This would be particularly interesting in combination with nsp7/8 (Ohyama et al., 2024, JACS Au).*

We thank the reviewer for this insightful and inspiring suggestion. Incorporating pseudoknot (PK) structures into our analysis—particularly the well-characterized PK in the 3'UTR (Sola et al., 2011)—represents a significant opportunity to bridge our biochemical findings with the viral life cycle. To address this, we have designed a 3'UTR PK substrate based on recently reported scaffolds (Ohyama et al., 2024).

Planned experiments:

(1) We will expand our initial binding assays (Figure 1) to include blunt-ended duplexes, hairpins, and the 3'UTR PK. This will establish a baseline for how Nsp13 recognizes these structurally distinct and physiologically critical templates.

(2) We will perform unwinding assays to determine whether Nsp13, in its isolated state, possesses the mechanical capability to resolve the complex tertiary interactions within a pseudoknot.

(3) Following the reviewer's insight, we will examine whether the addition of nsp7/8 is required to facilitate the unfolding of the 3'UTR PK.

Together, these experiments will allow us to assess whether Nsp13 is capable of managing one of the most challenging structural obstacles in the SARS-CoV-2 genome.

> ***Reviewer #2 (Public review):***
>
> *Summary:*
>
> *The authors are trying to broaden the understanding of SARS-CoV2 Nsp13 activity to show that a single viral protein can accomplish multiple functions. Additionally, they try to show that helicase function is not limited to ATP-driven, unidirectional unwinding.*
>
> *Strengths: The consistent application of statistics to triplicate experiments is a strength of the manuscript. The ToPif1 control in Figure S12 is a good control.*

We thank the reviewer for the insightful assessment and for highlighting the rigor of our experimental design, particularly our reliance on triplicate data with robust statistical validation and the inclusion of the ToPif1 control.

We are especially grateful for the detailed comments provided by the reviewer. We fully recognize that addressing these specific points is essential for strengthening the cogency of our conclusions and improving the overall rigor of the manuscript. These suggestions have provided us with a clear roadmap for further refining our experimental evidence and clarifying our mechanistic interpretations. Below, we respond point-by-point to the specific issues.

> *Weaknesses:*
>
> *(1) All the experiments except the one in Figure S2 use N-terminally His-tagged Nsp13. Because the N-terminal tag is known to have large effects on Nsp13 activity, this calls into question virtually all of the results in this manuscript.*

We thank the reviewer for raising this important concern regarding the potential influence of the N-terminal His tag on nsp13 activity. We have carefully considered this issue and provide the following lines of evidence to address it.

(1) We have generated a tag-free nsp13 variant and our preliminary characterization (Author response image 1) shows that it retains all key activities: ATP hydrolysis (comparable to His-tagged nsp13), both ATP-independent (Mg^{2+}-activated) and ATP-dependent unwinding, as well as chaperone activity to remodel stem-loops. These results demonstrate that while the His tag may modulate enzymatic efficiency, it does not create or abolish any specific biochemical function.

(2) We conducted a systematic survey of 27 published studies on SARS-CoV/SARS-CoV-2 nsp13 (Author response table 1). The results show that 17 out of 27 studies (63%) used affinity-tagged nsp13 without tag removal, including His, MBP, GST, and Strep tags.

(3) The only study that systematically compared different affinity tags (Adedeji et al., 2012) reported that GST-tagged nsp13 exhibited ~520-fold higher ATPase activity than His-tagged nsp13, demonstrating that the choice of affinity tag can affect enzymatic efficiency. However, both tagged versions retained all core enzymatic activities, including ATP hydrolysis and duplex unwinding. Importantly, no study has compared the full functional spectrum between His-tagged and tag-free nsp13. Our preliminary data suggest that the His tag may affect efficiency but does not alter the presence or absence of any specific activity.

Planned experiments:

We fully agree with the reviewer that a more systematic comparison would strengthen the conclusions. In the revision, we will include additional characterization of tag-free nsp13: (i) quantitative nucleic acid binding affinity, (ii) G4 unfolding efficiency, (iii) strand annealing activity. These experiments are currently underway.

In summary, while we acknowledge that the His tag may influence enzymatic efficiency, our key conclusions are supported by experiments with tag-free nsp13. We will add a discussion of these points and include additional tag-free nsp13 data in the revised manuscript.

> *(2) The ATP-independent, bidirectional duplex unwinding shown for short duplex substrates is reminiscent of the trapping of thermal fraying intermediates that have been reported for other helicases. Because they are only observed on short duplexes, do not require ATP, and are bidirectional, this does not suggest strand displacement as suggested in the manuscript. Instead, it suggests trapping of partially melted intermediates.*

We thank the reviewer for this insightful perspective. While the passive trapping of thermal fraying intermediates is a well-established model for non-catalytic protein-nucleic acid interactions, several lines of evidence suggest that nsp13 employs a more active, allosteric mechanism for ATP-independent remodeling.

(1) If nsp13 were merely a passive trap, increasing duplex stability should decrease unwinding. However, as shown in Figure S3, raising Mg^{2+} from 0 to 5 mM increases the DNA duplex Tm by ~10°C, yet nsp13's remodeling activity is markedly enhanced under the same conditions (Figure 2). This positive correlation between cation-induced substrate stabilization

and protein activation supports an active, protein-centered mechanism that overcomes the increased energetic barrier.

(2) The observed bidirectionality in ATP-independent remodeling does not simply imply a lack of polarity; rather, it can reflect nsp13's intrinsic chaperone function. In the absence of ATP, nsp13 binds the ss/ds junction (Figure 2F) and, in a Mg^{2+}-dependent manner, may use its binding energy to actively intercalate into the duplex. This mechanism is inherently symmetric for 3' and 5' overhangs, explaining bidirectional remodeling, while the absence of activity on blunt-ended substrates confirms the requirement for a pre-existing junction.

(3) The lack of activity on 24-bp substrates does not negate this remodeling mode but defines its energetic boundary. The binding energy released upon nsp13-nucleic acid interaction is sufficient to overcome the lower unwinding barrier of 12-16 bp duplexes, but insufficient to counteract the high stability and rapid re-annealing of a 24-bp duplex without the continuous mechanical power of ATP hydrolysis.

Planned Revision:

We thank the reviewer for prompting us to refine our mechanistic model. In the revision, we will add a dedicated discussion explicitly comparing the model of allosterically activated, binding-driven strand intrusion with the passive trapping model, incorporating the Tm data to strengthen our conclusions.

> *(3) Results that may be artifacts of unusual in vitro conditions are interpreted as if similar results will occur in the cell, where ATP is likely always present. Along those same lines, SARS-CoV-2 replicates in compartments of the endoplasmic reticulum, which would limit the ability of Nsp13 to access DNA substrates.*

We thank the reviewer for raising this important concern regarding the physiological relevance. We fully agree that *in vitro* conditions do not entirely recapitulate the complex intracellular environment, and we have been careful not to over-interpret our findings. Below we address the two specific issues raised:

(1) Regarding the ATP-independent activity, we acknowledge that ATP is abundant in healthy, actively replicating cells. However, during rapid viral replication, local ATP concentrations can fluctuate due to the high energy demand of the RTC as the template contains extensive secondary structures, which may lead to transient ATP depletion. Under such energy-limited conditions, Yu et al. (2025) demonstrated that ADP-bound nsp13 exhibits chaperone activity that destabilizes nucleic acid structures without ATP hydrolysis, and Dumm et al. (2025) reported that SARS-CoV-2 nsp13 resolves RNA stem-loops in an ATP-independent manner.

Even when ATP is abundant, the ATP-independent mode may enable rapid, local structural adjustments that bypass the kinetic delay of ATP binding and hydrolysis. As shown in Figure 1D, nsp13 exhibits high binding affinity for structured nucleic acids. In this scenario, nsp13 functions not as a processive motor but through a binding-driven mechanism, using the free energy of protein-nucleic acid interaction to transiently destabilize short duplexes or resolve local secondary structures such as G4s and stem-loops in an energy-efficient manner.

(2) Regarding DNA substrates, we fully agree that RNA is the physiological substrate for nsp13. However, DNA is a validated and widely accepted surrogate for mechanistic studies because DNA is more stable and easier to manipulate than RNA to yield the mechanistic insights. A systematic survey of 27 published nsp13 studies (Author response table 1) shows that 20 out of 27 (74%) used DNA substrates for at least some of their experiments. In our study, we used DNA primarily as a mechanistic probe and a stable control, and we validated all key conclusions on physiological RNA substrates, as shown in Figures 4, 5, 6, S7, S8, S10, S11 and S12.

Planned revisions: To address the reviewer's concerns more directly, we will revise the manuscript to include a discussion paragraph explicitly stating that the ATP-independent activity was observed under optimized *in vitro* conditions and may represent a latent remodeling capability that could be relevant under energy-limited conditions such as local ATP depletion during rapid replication. We will also clarify that DNA substrates were used as mechanistic probes and controls, and that all key findings were validated on physiological RNA substrates. We thank the reviewer for prompting us to strengthen the discussion of these important points.

> *(4) There is no evidence to support the conclusion that "Duplex DNA supports bidirectional remodeling via both ATP-dependent and ATP-independent mechanisms." 3'-5' duplex melting is limited to short duplexes and is ATP-independent, suggesting it may be due to trapping of thermal fraying intermediates by the ssDNA binding Nsp13. The ATP-dependent and ATP-independent melting on the substrates with the 3'-overhang are the same, suggesting that ATP-dependent melting does not occur on this substrate, which would indicate that bidirectional ATP-dependent translocation does not occur.*

We are grateful to the reviewer for this critical evaluation of our mechanistic claims. We agree that our initial statement regarding bidirectional ATP-dependent remodeling was imprecise and not fully supported by the data. As the reviewer correctly notes, the similar unwinding efficiency on 3'-overhang substrates regardless of ATP presence indicates that ATP hydrolysis does not drive 3'→5' translocation, which is consistent with nsp13's known 5'→3' motor polarity. The observed 3'→5' activity is therefore more accurately described as an ATP-independent remodeling event, not ATP-dependent unwinding.

We will revise the Discussion and relevant Results sections to clarify the nature of this bidirectional activity. Specifically, the sentence:

"Duplex DNA supports bidirectional remodeling via both ATP-dependent and ATP-independent mechanisms..."will be corrected to: "Duplex DNA supports bidirectional remodeling via ATP-independent mechanisms."

We will also explicitly state that while nsp13 requires ATP for long-range, processive 5'→3' helicase activity, its remodeling/chaperone function is inherently bidirectional and powered by the free energy of binding to the ss/ds junction, rather than by ATP-driven mechanical work.

> *(5)-The description of ATP-independent unwinding as having "limited processivity," is likely not accurate. These experiments were multiturnover reactions with very high Nsp13 concentrations and no protein trap to ensure single turnover conditions. Because the reactions were multi-turnover, no information about the processivity of Nsp13 can be obtained. On the contrary, it seems likely that the product formed over the 30-minute reaction with a vast excess of Nsp13 is due to binding and dissociation of multiple Nsp13 molecules instead of processive translocation by a single enzyme.*

We thank the reviewer for this important correction. We fully agree that our use of the term "processivity" was technically imprecise. Processivity strictly defines the distance a single enzyme translocates during one binding event, which our multi-turnover assays (with high nsp13 concentrations and no protein trap) were not designed to measure. Our results specifically demonstrate that the ATP-independent remodeling mode is highly sensitive to duplex length, with efficiency declining sharply as the duplex lengthens. To reflect the experimental data more faithfully, we have replaced "processivity" with more accurate descriptors throughout the manuscript.

Planned revisions:

(1) Original: "The ATP-independent unwinding mode, however, has limited processivity." Revised: "The ATP-independent unwinding mode, however, exhibits a steep decline in efficiency as the duplex length increases."

(2) Original: "...an ATP-independent, cation-activated mode with limited processivity." Revised: "...an ATP-independent, cation-activated mode specialized for localized structural remodeling"

(3) Original: "...primes Nsp13 for basal strand remodeling but supports only limited processivity." Revised: "...primes Nsp13 for basal strand remodeling but is insufficient for the sustained unwinding of extended duplexes."

(4) Original: "...primes Nsp13 for low-processivity strand displacement." Revised: "...primes Nsp13 for short-range strand displacement rather than long-range processive unwinding."

We believe these changes clarify that the ATP-independent mode acts as a molecular chaperone for local obstacles (like G4 or short stems) rather than a motor for long-range translocation. We thank the reviewer for helping us improve the precision of our description.

> *(6) G4s are much more stable at cellular K+ concentrations than they are at 20 mM K+. As such, Nsp13's ability to unfold a G4 in the absence of ATP may be diminished or eliminated at a physiological K+ concentration.*

We thank the reviewer for this critical point regarding physiological ion concentrations. We agree that K^+ significantly stabilizes G4 structures, which may raise the energy barrier for ATP-independent remodeling.

Planned experiments:

To address this, we will perform salt titration assays (up to 150 mM KCl) to evaluate the robustness of nsp13's G4 unfolding activity under more physiological ionic conditions. We will also measure the melting temperature of our G4 substrates across this K^+ range to correlate structural stability with enzymatic efficiency.

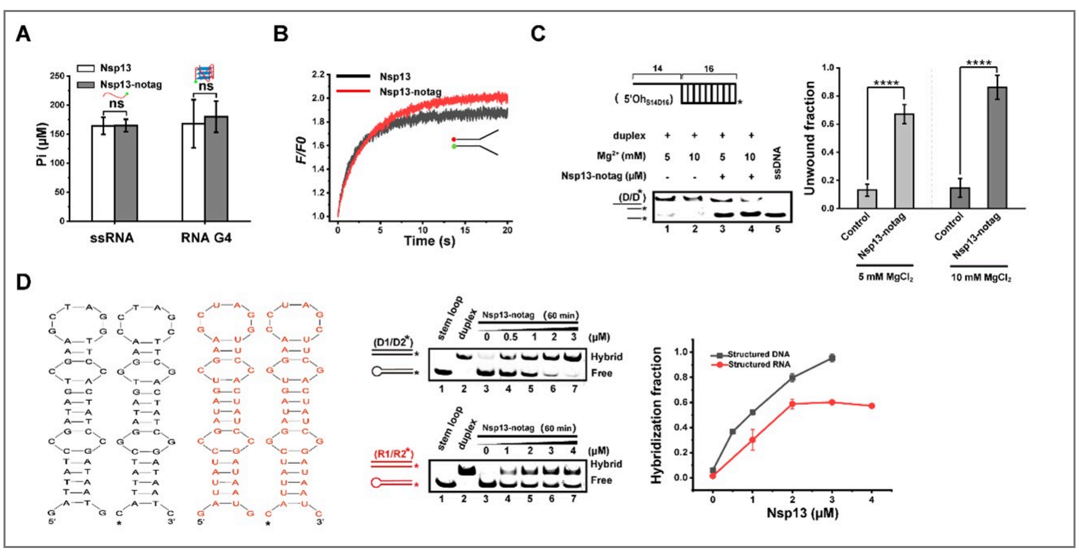

Author response image 1. Preliminary characterization of tag-free Nsp13 enzymatic activities. (A) Comparison of ATPase activity between His-tagged and tag-free Nsp13 in the presence of ssRNA or RNA G4. (B) Raw fluorescence data from stopped-flow FRET analysis of ATP-dependent unwinding (16-bp fork DNA, 2 mM Mg^{2+}, 2 mM ATP). F/F_0 represents FAM fluorescence normalized to initial DNA intensity. (C) ATP-independent DNA duplex remodeling (data reproduced from Figure S2). (D) Chaperone activity of tag-free Nsp13 on DNA and RNA stem-loops.

No.	Paper (First author & year)	Final Tag Status	Monovalent Cation in Unwinding Buffer	Substrate Type
1	Ivanov et al., JVI (2004)	MBP (retained)	20 mM HEPES-KOH	RNA + DNA
2	Lee et al., NAR (2010)	His (retained)	50 mM NaCl	DNA
3	Adedeji et al., PLoS ONE (2012)	GST / His / MBP (all retained)	20 mM NaCl	DNA (mainly) + RNA
4	Adedeji & Lazarus, mSphere (2016)	Strep (retained)	20 mM NaCl	RNA + DNA
5	Jia et al., NAR (2019)	His (retained)	20 mM NaCl	DNA
6	Jang et al., Sci Rep (2020)	His (retained)	50 mM NaCl	RNA + DNA
7	Shu et al., Virol Sin (2020)	MBP (retained)	50 mM NaCl	RNA
8	Mickolajczyk et al., Biophys J (2021)	His (cleaved, PreScission)	40 mM KCl (bulk) / 20 mM KCl (tweezers)	RNA+DNA
9	Chen et al., NSMB (2022)	His (cleaved, PreScission)	None unwinding assay	
10	Yazdi et al., ACS Infect Dis (2022)	His (retained)	0 mM (optimized, NaCl removed)	ATPase only (no unwinding)
11	Corona et al., ACS Pharmacol Transl Sci (2022)	His (cleaved, TEV)	50 mM NaCl	DNA
12	Lu et al., Antiviral Res (2022)	His (retained)	20 mM NaCl	DNA
13	Yue et al., BBRC (2022)	His + Myc (retained)	40 mM KCl	RNA
14	Grimes et al., mBio (2023)	His (cleaved, PreScission)	40 mM KCl	RNA + DNA
15	Yu et al., BBRC (2023)	His (retained)	25 mM NaCl	DNA
16	Sommers et al., JBC (2023)	His + FLAG (N-terminal His cleaved)	20 mM NaCl	RNA (mainly) + DNA
17	Maio et al., PNAS (2023)	Strep II (retained)	100 mM KCl	RNA + DNA
18	Marx et al., NAR (2023)	His (cleaved, PreScission)	20 mM KCl	DNA (ssDNA + dsDNA)
19	Inniss et al., SLAS Discov (2024)	His (cleaved, TEV)	50 mM NaCl	RNA
20	Sales et al., IJMS (2024)	His (retained)	10 mM KCl	DNA
21	Soper et al., ACS Chem Biol (2024)	His (cleaved, TEV)	20 mM KCl	DNA
22	Hao et al., Chem Biomed Imaging (2024)	His-SUMO (cleaved, PreScission)	50 mM NaCl	DNA
23	Park et al., JBC (2025)	His (retained)	50 mM NaCl	DNA (mainly) + RNA
24	Yu et al., NAR (2025)	His (retained)	20 mM NaCl	DNA (mainly) + RNA
25	Dumm et al., NAR (2025)	His + FLAG (N-terminal His cleaved)	20 mM NaCl	RNA
26	Castro et al., IJMS (2026)	His (retained)	20 mM NaCl	DNA
27	Mingroni et al., JBC (2026)	6xHis-ZBasic (retained)	20 mM NaCl	DNA

Author response table 1. **Summary of affinity tags, monovalent salt concentrations, and substrate types used in 27 published SARS-CoV/SARS-CoV-2 nsp13 studies**

References:

(1) Ivanov KA, Thiel V, Dobbe JC, van der Meer Y, Snijder EJ, Ziebuhr J. Multiple enzymatic activities associated with severe acute respiratory syndrome coronavirus helicase. J Virol. 2004 Jun;78(11):5619-32.

(2) Lee NR, Kwon HM, Park K, Oh S, Jeong YJ, Kim DE. Cooperative translocation enhances the unwinding of duplex DNA by SARS coronavirus helicase nsP13. Nucleic Acids Res. 2010 Nov;38(21):7626-36.

(3) Adedeji AO, Marchand B, Te Velthuis AJ, Snijder EJ, Weiss S, Eoff RL, Singh K, Sarafianos SG. Mechanism of nucleic acid unwinding by SARS-CoV helicase. PLoS One. 2012;7(5):e36521. doi: 10.1371/journal.pone.0036521.

(4) Adedeji AO, Lazarus H. Biochemical Characterization of Middle East Respiratory Syndrome Coronavirus Helicase. mSphere. 2016 Sep 7;1(5):e00235-16.

(5) Jia Z, Yan L, Ren Z, Wu L, Wang J, Guo J, Zheng L, Ming Z, Zhang L, Lou Z, Rao Z. Delicate structural coordination of the Severe Acute Respiratory Syndrome coronavirus Nsp13 upon ATP hydrolysis. Nucleic Acids Res. 2019 Jul 9;47(12):6538-6550.

(4) Jang KJ, Jeong S, Kang DY, Sp N, Yang YM, Kim DE. A high ATP concentration enhances the cooperative translocation of the SARS coronavirus helicase nsP13 in the unwinding of duplex RNA. Sci Rep. 2020 Mar 11;10(1):4481.

(5) Shu T, Huang M, Wu D, Ren Y, Zhang X, Han Y, Mu J, Wang R, Qiu Y, Zhang DY, Zhou X. SARS-Coronavirus-2 Nsp13 Possesses NTPase and RNA Helicase Activities That Can Be Inhibited by Bismuth Salts. Virol Sin. 2020 Jun;35(3):321-329.

(6) Mickolajczyk KJ, Shelton PMM, Grasso M, Cao X, Warrington SE, Aher A, Liu S, Kapoor TM. Force-dependent stimulation of RNA unwinding by SARS-CoV-2 nsp13 helicase. Biophys J. 2021 Mar 16;120(6):1020-1030.

(7) Chen J, Wang Q, Malone B, Llewellyn E, Pechersky Y, Maruthi K, Eng ET, Perry JK, Campbell EA, Shaw DE, Darst SA. Ensemble cryo-EM reveals conformational states of the nsp13 helicase in the SARS-CoV-2 helicase replication-transcription complex. Nat Struct Mol Biol. 2022 Mar;29(3):250-260.

(8) Yazdi AK, Pakarian P, Perveen S, Hajian T, Santhakumar V, Bolotokova A, Li F, Vedadi M. Kinetic Characterization of SARS-CoV-2 nsp13 ATPase Activity and Discovery of Small-Molecule Inhibitors. ACS Infect Dis. 2022 Aug 12;8(8):1533-1542.

(9) Corona A, Wycisk K, Talarico C, Manelfi C, Milia J, Cannalire R, Esposito F, Gribbon P, Zaliani A, Iaconis D, Beccari AR, Summa V, Nowotny M, Tramontano E. Natural Compounds Inhibit SARS-CoV-2 nsp13 Unwinding and ATPase Enzyme Activities. ACS Pharmacol Transl Sci. 2022 Apr 1;5(4):226-239.

(10) Lu L, Peng Y, Yao H, Wang Y, Li J, Yang Y, Lin Z. Punicalagin as an allosteric NSP13 helicase inhibitor potently suppresses SARS-CoV-2 replication in vitro. Antiviral Res. 2022 Oct;206:105389.

(11) Yue K, Yao B, Shi Y, Yang Y, Qian Z, Ci Y, Shi L. The stalk domain of SARS-CoV-2 NSP13 is essential for its helicase activity. Biochem Biophys Res Commun. 2022 Apr 23;601:129-136.

(12) Grimes SL, Choi YJ, Banerjee A, Small G, Anderson-Daniels J, Gribble J, Pruijssers AJ, Agostini ML, Abu-Shmais A, Lu X, Darst SA, Campbell E, Denison MR. A mutation in the coronavirus nsp13-helicase impairs enzymatic activity and confers partial remdesivir resistance. mBio. 2023 Aug 31;14(4):e0106023.

(13) Yu J, Im H, Lee G. Unwinding mechanism of SARS-CoV helicase (nsp13) in the presence of Ca2+, elucidated by biochemical and single-molecular studies. Biochem Biophys Res Commun. 2023 Aug 6;668:35-41.

(14) Sommers JA, Loftus LN, Jones MP 3rd, Lee RA, Haren CE, Dumm AJ, Brosh RM Jr. Biochemical analysis of SARS-CoV-2 Nsp13 helicase implicated in COVID-19 and factors that regulate its catalytic functions. J Biol Chem. 2023 Mar;299(3):102980.

(15) Maio N, Raza MK, Li Y, Zhang DL, Bollinger JM Jr, Krebs C, Rouault TA. An iron-sulfur cluster in the zinc-binding domain of the SARS-CoV-2 helicase modulates its RNA-binding and -unwinding activities. Proc Natl Acad Sci U S A. 2023 Aug 15;120(33):e2303860120.

(16) Marx SK, Mickolajczyk KJ, Craig JM, Thomas CA, Pfeffer AM, Abell SJ, Carrasco JD, Franzi MC, Huang JR, Kim HC, Brinkerhoff H, Kapoor TM, Gundlach JH, Laszlo AH. Observing

inhibition of the SARS-CoV-2 helicase at single-nucleotide resolution. Nucleic Acids Res. 2023 Sep 22;51(17):9266-9278.

(17) Inniss NL, Rzhetskaya M, Ling-Hu T, Lorenzo-Redondo R, Bachta KE, Satchell KJF, Hultquist JF. Activity and inhibition of the SARS-CoV-2 Omicron nsp13 R392C variant using RNA duplex unwinding assays. SLAS Discov. 2024 Apr;29(3):100145.

(18) Sales AH, Fu I, Durandin A, Ciervo S, Lupoli TJ, Shafirovich V, Broyde S, Geacintov NE. Variable Inhibition of DNA Unwinding Rates Catalyzed by the SARS-CoV-2 Helicase Nsp13 by Structurally Distinct Single DNA Lesions. Int J Mol Sci. 2024 Jul 19;25(14):7930.

(19) Soper N, Yardumian I, Chen E, Yang C, Ciervo S, Oom AL, Desvignes L, Mulligan MJ, Zhang Y, Lupoli TJ. A Repurposed Drug Interferes with Nucleic Acid to Inhibit the Dual Activities of Coronavirus Nsp13. ACS Chem Biol. 2024 Jul 19;19(7):1593-1603.

(20) Hao W, Hu X, Chen Q, Qin B, Tian Z, Li Z, Hou P, Zhao R, Balci H, Cui S, Diao J. Duplex Unwinding Mechanism of Coronavirus MERS-CoV nsp13 Helicase. Chem Biomed Imaging. 2024 Dec 19;3(2):111-122.

(21) Park J, Jeong YJ, Chauhan K, Koh HR, Kim DE. ATPase-dependent duplex nucleic acid unwinding by SARS-CoV-2 nsP13 relies on facile binding and translocation along single-stranded nucleic acid. J Biol Chem. 2025 Jul;301(7):110373.

(24) Yu J, Im H, Cho H, Jeon Y, Lee JB, Lee G. A novel ADP-directed chaperone function facilitates the ATP-driven motor activity of SARS-CoV helicase. Nucleic Acids Res. 2025 Jan 24;53(3):gkaf034.

(25) Dumm AJ, Zheng AY, Butler TJ, Kulikowicz T, George JC, Bombard PT, Sommers JA, Ding J, Brosh RM Jr. SARS-CoV-2 point mutations are over-represented in terminal loops of RNA stem-loop structures that can be resolved by Nsp13 helicase in a unique manner with respect to nucleotide dependence. Nucleic Acids Res. 2025 May 22;53(10):gkaf447.

(26) Castro JM, Slack RL, Ong YT, Zhang H, Gifford LB, Courouble VV, Aiken RM, Shankar V, O'Leary TR, Griffin PR, Lan S, Du Y, Fu H, Sarafianos SG. Stalling the Enemy: Targeting Nsp13 for Next-Generation SARS-CoV-2 Antivirals. Int J Mol Sci. 2026 Mar 11;27(6):2587.

(27) Mingroni MA, Enney BM, Malsick LE, Geiss BJ. Motif V is an allosteric couple between the SARS-CoV-2 nsp13 nucleotide triphosphatase and helicase active sites. J Biol Chem. 2026 Mar;302(3):111198.

https://doi.org/10.7554/eLife.110731.1.sa0